Thesis

Electronic States of Molecular Compound, (DI-DCNQI)$_2$M, (M = Li, Ag, Cu), and Doped System, (DMe-DCNQI)$_2$Li$_{1-x}$Cu$_x$

Ko-ichi Hiraki

Department of Functional Molecular Science,
School of Mathematical and Physical Science,
Graduate University for Advanced Studies

1996

Preface

The author is interested in organic conductors based on DCNQI, which has provided one-dimensional electronic structure and a variety of electronic phases. In this thesis, the novel electronic states of DCNQI-M system have been searched for by 1) changing the intercolumn interaction and band width, and 2) controlling the filling of the π band of DMe-DCNQI columns through the Cu doping to the nearly pure one-dimensional electronic system. The Cu doping is expected to cause some change in filling of the band and generate three-dimensional nature through hybridization of the Cu 3d orbital with the π band. The electronic states were investigated by resistivity, ρ, magnetic susceptibility, χ and ^{1}H- and ^{13}C-NMR measurements. The topics of 1) and 2) are described in chapters 3 and 4, respectively.

Acknowledgment

The present work has been carried out under the supervision of Prof. Kaz. Kanoda at the Graduate Univ. for Advanced Studies and the Institute for Molecular Science (GUAS-IMS). The author would like to express his sincere thanks to Prof. Kaz. Kanoda for his continuous encouragement and guidance. The author wishes to thank all the members of the Kanoda research group, Dr. Y. Nakazawa (GUAS-IMS), Dr. A. Kawamoto (Ochanomizu Univ.), Messrs. K. Miyagawa (IMS), H. Taniguchi (GUAS-IMS) for their valuable discussions, comments and suggestions. The author also thanks Prof. R. Kato, Dr. S. Aonuma, Mr. Y. Kashimura (ISSP Univ. of Tokyo), Dr. M. Tamura (Toho Univ. and ISSP Univ. of Tokyo) and Prof. H. Sawa (Chiba Univ. and ISSP Univ. of Tokyo) for useful comments and discussions on the sample preparation, crystal structures and transport properties and magnetism. The author thanks Dr. T. Miyazaki (NRIM and JRCAT), Prof. K. Terakura (JRCAT) and Prof. K. Yonemitsu (IMS) for enlightening discussions on the band structures and theoretical aspects. The author also thanks Prof. Y. Nogami (Okayama Univ.) for useful comments and suggestions on the *X*-ray experiments. Thanks are also due to Messrs. K. Kato and T. Takayama (IMS) for their technical supports in low temperature experiments. The author wishes to thank Prof. T. Takahashi and the members of Takahashi research group (Gakushuin Univ.) for continuous encouragement and invaluable discussion. The author feels thankful to the Japan Society for the Promotion of Science for financial support.

Abbreviations

1D (2D, 3D)	one (two, three) dimensional
TTF	tetrathiafulvalene
TCNQ	tetracyanoquinodimethane
TMTTF	tetramethyltetrathiafulvalene
TMTSF	tetramethyltetraselenafulvalene
BEDT-TTF	bis(ethylenedithio)tetrathiafulvalene
DCNQI	dicyanoquinonediimine
Me	methyl group
CL	charge localization
SP	spin Peierls
CDW	charge density wave
SDW	spin density wave
NMR	nuclear magnetic resonance
LUMO	the lowest unoccupied molecular orbital
AF	antiferromagnetic
ρ	electrical resistivity
χ	magnetic susceptibility
g	g-value of electron
K	NMR shift
T_1^{-1}	nuclear spin lattice relaxation rate

γ	gyromagnetic ratio of nucleus
$\vec{I}$	nuclear spin number
$\vec{S}$	electron spin number
μ_B	Bohr magneton

Contents

Chapter 1.

General Introduction

1-1 Organic conductors
1-2 DCNQI-M complexes
1-3 Scope of the present study
References

1-1 Organic conductors

There are increasing interests in the electronic properties of organic or molecular conductors. The features of the organic compounds are summarized as follows,

1. controllability of the electronic properties by molecular modification
2. low-dimensionality (1D, quasi-1D, 2D)
3. strong correlation of conduction electrons
4. strong electron lattice interaction.

In this chapter, the historical aspects of organic conductors are described briefly.

The conducting charge transfer salt consists of a donner subsystem and an acceptor one, either of both which are responsible for electronic conduction. When the molecules form a stacking structure, the overlap of the π orbital of the molecules form a 1D conduction band. TTF-TCNQ (Fig. 1-1-1) was an epoch-making charge transfer organic compound which was first synthesized in 1970[1]. The planer molecules, TTF and TCNQ, stack to form segregated 1D columns along the crystallographic *b* axis[2]. This compound has high electrical conductivity along the *b* axis[2] even at room temperature. With decreasing temperature, the high conductivity increases further more than that expected in the normal metal (Fig. 1-1-2) [3]. At 53 K, the conductivity forms a peak and at lower temperatures, it decreases rapidly. The peak of conductivity was considered to come from fluctuations of the superconductivity[4]. But the possibility of the high temperature superconductivity was roled out later. The anomaly is now understood as a metal-insulator transition with lattice distortion, namely the Peierls transition[5]. TTF-TCNQ introduced a new phenomena of CDW, which is a new mode of the Fermi surface

instability in the 1D electronic system.

TMTTF and TMTSF molecules are shown in Fig. 1-1-3. They form a charge transfer complexes with nonmagnetic counter anions, X (X=PF_6, AsF_6, ClO_4, Br, *etc*). The electronic conduction in TTF-TCNQ is carried by two kinds of conducting columns, TTF (hole conduction) and TCNQ (electron conduction). On the other hand, the conduction in $(TMTTF/TMTSF)_2X$ (abbreviated to TM_2X) is carried only by the TMTTF/TMTSF stack (hole conduction) as shown in Fig. 1-1-4[6]. Since the valency of the TM molecule is +1/2, the filling of the quasi-1D π electronic band is turned out to be quarter. Many member in the TM_2X family behave metallic at high temperatures while they undergo metal-insulator transition or charge localization (CL) at low temperatures[7]. In the insulating states of this system, the collective modes of charge or spin has been frozen in a different manner from that of TTF-TCNQ. The typical Pressure-Temperature phase diagram of TM_2X is shown in Fig. 1-1-5. The physics of this phase diagram is considered as follows. As seen in the crystal structure (Fig. 1-1-4), we can see the two fold periodic potential by the location of the anion, X (in this case, X=PF_6), along the column axis. The anion potential folds the Brillouin zone. The band structure is changed from quarter filling to half filling, effectively. In presence of the large Coulomb repulsion, U, the system can become a Mott insulator. This is considered to be the case in $(TMTTF)_2PF_6$, for example. At lower temperatures, the local spins, appeared at CL transition, form a long-range singlet-like state with lattice distortion along the column axis in this salt. The ground state is the non magnetic spin-Peierls (SP) state. Applying pressure transfer the system toward the right-hand side in the phase diagram[8] with a charge of the ground state to SDW state due to liftinng of dimensionality. Replacing the sulfur atoms in TMTTF to selenium,

and changing the anion, X, are considered to have the same effect as application of pressure. The most remarkable fact is that the superconducting state is situated in the neighbor of the SDW state. In 1979, it was reported that $(TMTSF)_2PF_6$ shows superconductivity around 1 K under a pressure of 12kbar[9]. This is the first report of the superconductivity in the organic compounds. In 1980, $(TMTSF)_2ClO_4$ was reported to shows superconductivity at ambient pressure[10]. But most of TM_2X systems undergo the metal-insulator transition at ambient pressure due to the Fermi surface instability of the 1D electronic system.

The BEDT-TTF (ET) molecule (Fig. 1-1-6) opened a way to wide variation of molecular arrangement in two dimension, where nesting of Fermi surface is not effective [11]. A typical crystal structure of ET_2X are shown in Fig. 1-1-7, where the case of $X=Cu(NCS)_2$ is depicted[12]. The ET molecule and X form 2D conducting and insulating sheet, respectively. This layered structure gives quasi 2D electronic structure, which is a strong contrast to the case of TM_2X and tends to suppress Peierls or SDW transition. In fact, many of ET_2X remain metallic down to lower temperatures[13]. The salt with $X=Cu[N(CN)_2]Br$ has the highest T_C among the organic superconductors to date (T_C =11.6 K)[14].

The investigations of metal complexes of DCNQI (DCNQI-M) started in 1986[15]. Although superconductivity has not yet observed, the DCNQI-M system introduced novel physical interests in terms of the electron correlation and π-d hybridization inherent in term. The properties of DCNQI-M are described in the next chapter.

1-2 DCNQI-M complexes

DCNQI molecule is shown in Fig. 1-2-1. This is an organic π acceptor molecule, which is uniformly stacked along the *c* axis in the crystal, forming 1D columns. The metallic ions, M (M=Li, Ag, Cu), are coordinated in D_{2d} distorted tetrahedral fashion to the N atoms of CN groups of DCNQI molecules[16]. The M complexes of DCNQI, $(DCNQI)_2M$ or DCNQI-M, have the same crystal symmetry with the space group, $I4_1/a$, irrespectively of the kind of M or the substitution group, R^1/R^2[17]. In 1986, A. Aumüllar *et al.* reported that $(DMe\text{-}DCNQI)_2Cu$ (R^1/R^2=Me) remains metallic down to liquid helium temperature in spite of the low-dimensional structure[15]. The Peierls instability due to the one dimensionality was not observed. Their report is the beginning of the study of the DCNQI-Cu system. The stability of the metallic state in $(DMe\text{-}DCNQI)_2Cu$ comes from the hybridization of Cu 3d orbital and 1D organic π band[18].

In this chapter, the electronic properties of DCNQI-M complexes are described from the viewpoint of the π-d hybridization* .

$(DMe\text{-}DCNQI)_2Li$, $(DMe\text{-}DCNQI)_2Ag$

The electronic states of the complexes with monovalent metal ions are insensitive to the choice of Li or Ag become the electrons of Li and Ag do not contribute to the electronic

---

* The results in the figures 1-2-2, 1-2-4 and 1-2-6 in this chapter were obtained by the present author. All of them reproduced the earlier results [42].

properties[19]. The conduction band in the Li/Ag salt of DMe-DCNQI, DMe-Li/Ag is constructed by the DMe-DCNQI columns and therefore have strong 1D characters. In Fig. 1-2-2, temperature dependence of ρ and χ of DMe-Li (a) and DMe-Ag (b), is shown. DMe-Li/DMe-Ag behaves metallic at higher temperature while it becomes insulating at lower temperatures. Since Li/Ag is monovalent in the crystal, the valency of DMe-DCNQI is -1/2. Therefore the filling of the 1D π band is quarter with the Fermi wave vector, $k_F=c^*/4$. The ground state is non magnetic Peierls (or spin-Peierls) state with lattice distortion of $2k_F$ CDW[20]. The gradual change of the resistivity can be explained in terms of pseudo gap due to the fluctuations of $2k_F$ CDW and/or freezing of $4k_F$ CDW which is suggested by the *X*-ray diffuse scattering[20].

(DMe-DCNQI)$_2$Cu

The mixed valent Cu ions interconnect the DCNQI 1D π bands through the 3d orbital at Fermi level[18]. The average valence of Cu is known to be close to +4/3; Cu^{+}:Cu^{2+}~2:1[18,21,22]. The valence of the DCNQI molecule turned out to be ~-2/3 [18,27]. Therefore the filling of the 1D π band is ~1/3. The properties of Cu salt of DCNQI is quite sensitive to pressure. The temperature-pressure phase diagram of DCNQI-Cu is shown in Fig. 1-2-3. (DMe-DCNQI)$_2$Cu behaves metallic down to low temperatures at ambient pressure as shown in Fig. 1-2-2 (c), while under ~300bar the insulating state is induced at 70-200 K, depending on the pressure[23]. In the insulating phase, a superlattice with three fold period [24,25] and a charge separation of the Cu ion like $Cu^{2+}Cu^{1+}Cu^{1+}Cu^{2+}Cu^{1+}Cu^{1+}$ occur simultaneously along the *c* axis[26]. In the

metallic state, the spin susceptibility, χ, is not sensitive to temperature like Pauli paramagnetism (Fig. 1-2-2(c)), while in the insulating phase the Curie-Weiβ type of magnetism is observed, which is carried by the Cu^{2+} spins (Fig. 1-2-4). At lower temperatures, typically below 10 K, the Cu^{2+} spins order antiferromagnetically[26-28]. The replacement of the substitution group, R^1/R^2, has the same effect as application of pressure[31]. DMe(d)/DBr/DCl-Cu undergoes the metal-insulator transition even at ambient pressure[29,30]. The metal insulator transition of the Cu salts is understood as a cooperative phenomena of Peierls transition in the π band and Mott transition in the d-like band[31].

(DI-DCNQI)$_2$Cu

(DI-DCNQI)$_2$Cu, which was first synthesized by Hünig *et al.*, has the same crystal symmetry as DMe-M and also behaves metallic down to low temperatures[32]. The electronic properties of the DI-Cu are different from those of the DMe-Cu in the following respects,

1. anisotropy of resistivity, $\rho_\perp/\rho_\parallel$, in DI-Cu ~3 is less than that of DMe-Cu (~10) [33] (Fig. 1-2-5)
2. critical pressure of the metal-insulator transition is markedly larger in DI-Cu (~15kbar) than the DMe-Cu (~0.3kbar) [33] (Fig. 1-2-4)
3. χ of the DI-Cu is about twice as large as that of DMe-Cu and forms a broad peak at around 110 K[34] (Fig. 1-2-6).

The population of LUMO on the iodine sites in DI-DCNQI is much larger than on the

methyl sites in DMe-DCNQI. The facts of 1. and 2. may be explained by the 3D nature caused by the direct LUMO-LUMO interaction through the iodine sites in DI-Cu[33]. The fact of 3. suggests enhancement of the electron correlation effect in this system. The band width is predicted to be narrower in DI-Cu by first principle band calculation[35]. Estimate of the intracolumn transfer integrals based on the molecular orbital calculation also indicates narrower 1D π band in the DI-DCNQI column[33].

1-3 Scope of the present study

In the real materials, there is some degree of three dimensionality due to the intercolumn interaction even when it is called the 1D conductor. For example, the ratio of the transfer integrals in three directions in TM_2X is ~1:10:100 (t_a:t_c:t_b)[37]. As for $(DMe\text{-}DCQI)_2Cu$, the ratio is ~1:10 (t_c:t_a)[38]. The purpose of the present study is to synthesize and examine new electronic states caused by changing the magnitude of the intercolumn interaction and/or band filling of the 1D electronic system. The M (Li, Ag, Cu) salt of DCNQI is advantageous to perform the present study by the following reasons.

- Easy to control the intercoulmn interaction by changing the substitution group, R^1/R^2.
- Same crystal symmetry between the salts with monovalent Li/Ag and mixed valent Cu (~1.3+). The crystal symmetry is also independent of R^1/R^2
- As for Cu salt, there is intercolumn interaction via the 3d orbitals of Cu ions.

It seems that the replacing the substituents, Me to I, increases the intercolumn interaction through the LUMO on iodine sites and decreases the intracolumn transfer

integral[33,35]. The DI-systems is expected to be more three dimensional and highly correlated than DMe-system. The conducting and magnetic properties of 1D electronic system constructed by DI-DNQI columns are described in chapter 3. The Ag and Li salts with DI-DCNQI, DI-Ag and DI-Li, have been newly synthesized in the present study. DI-Li/DI-Ag is expected to afford nearly pure π electronic systems constructed by the original DI-DCNQI columns. In the chapter 3-2, the author has synthesized DMe-M and DI-M systems systematically and characterized by ρ and χ measurements. The detailed electronic structures have been studied by $^{1}H/^{13}C$-NMR measurements in chapters from 3-3 to 3-6. In chapter 3-6, the metallic state of DI-Cu are discussed with the viewpoint of the hybridization between the Cu 3d orbital and π band.

In the chapter 4, an attempt of carrier doping to the 1D electronic system is described. The author aimed at controlling the filling of DMe-DCNQI 1D π band by changing the average valence of M with alloying of M with different valences. The ground state of undoped DMe-Li is a nonmagnetic insulator associated with freezing of $2k_F$ CDW[20]. It is expected that the Cu doping to the Li site in DMe-Li causes some change in the filling of the 1D π band and also generates the 3D character through participation of the Cu 3d orbital to the electronic band. The doped system, $(DMe\text{-}DCNQI)_2Li_{1-x}Cu_x$, were synthesized systematically and characterized by the measurements of ρ and χ, that are described in the chapters 4-1, 4-2 and 4-3. The detailed of the systems by ^{13}C-NMR measurements is described in chapter 4-4.

References

1. F. Full *et al.*, J. Chem. Soc. Chem. Commun. **1970**, 1453 (1970); J. P. Ferraris *et al.*, J. Am. Chem. Soc. **95**, 948 (1973)
2. T. E. Phillips *et al.*, J. Chem. Soc. Chem. Commun. **1973**, 471 (1973); T. J. Kistenmacher *et al.*, Acta Cryst. **B30**, 763 (1974)
3. M. J. Cohen *et al.*, Phys. Rev. **B10**, 1928 (1977); S. Etemd Phys. Rev. **B13**, 2254 (1976), T. Ishiguro *et al.*, J. Phys. Soc. Jpn. **41**, 351 (1976)
4. L. B. Coleman *et al.*, Solid State Commun. **12**, 1125 (1973)
5. "High Conducting One-Dimensional Solid" ed. J. T. Devreese et al. (Plenum, 1979)
6. D. Jerome, "Organic Conductors", ed. Jean-Pierre Farges (Marcel Dekker, New York, 1994) p. 420.
7. C. Coulon *et al.*, J. Physique **43**, 1059 (1982)
8. K. Mortensen *et al.*, Phys. Rev. Lett. **46**, 1234 (1981)
9. D. Jerome *et al.*, J. Phys. Lett. (paris), **41**, L95 (1980)
10. K. Bechgaard *et al.*, Phys. Rev. Lett. **46**, 852 (1981)
11. M. Mizuno *et al.*, J. Chem. Soc. Chem. Commun. **1978**, 18 (1978)
12. H. Urayama *et al.*, Chem Lett. **1988**, 55 (1988)
13. G. Saito *et al.*, Solid State Commun. **42**, 557 (1982)
14. A. M. Kini *et al.*, Inorg. Chem. **29**, 2555 (1990)
15. A. Aumüller *et al.*, Angew. Chem. Int. Ed. Engel. **25**, 740 (1986)
16. R. Kato *et al.*, Chem. Lett. **1987**, 1579 (1987)
17. R. Kato *et al.*, J. Am. Chem. Soc. **111**, 5224 (1989)

18. H. Kobayashi *et al.*, Phys. Rev. **B47**, 3500 (1993)

19. H. J. Gross *et al.*, J. Phys. France **50**, 2347 (1989)

20. R. Moret *et al.*, J. Phys. France **49**, 1925 (1988); M. Meneghetti *et al.*, Synth. Met. **41-43**, 1775 (1991)

21. I. H. Inoue *et al.*, Phys. Rev. **B45**, 5828 (1992)

22. T. Takahashi *et al.*, unnpublished

23. S. Tomic *et al.*, Europhys. Lett. **5**, 553 (1988)

24. A. Kobayashi *et al.*, Solid State Commun. **64**, 45 (19879

25. H. Sawa *et al.*, J. Phys. Soc. Jpn. **62**, 2224 (1993)

26. K. Hiraki *et al.*, J. Phys. Soc. Jpn. **64**, 2203 (1995)

27. H. Kobayashi *et al.*, J. Phys. Solids **51**, 533 (1990)

28. M. Tamura *et al.*, J Phys. Soc. Jpn. **63**, 425 (1994)

29. R. Kato *et al.*, Solid State Commun. **85**, 831 (1993)

30. S. Aonuma *et al.*, Chem. Lett. **1993**, 513 (1993)

31. H. Fukuyama; Prog. Theor. Phys. **113**, 125 (1993)

32. P. Erk *et al.*, Adv. Matter **3**, 311 (1991)

33. Y. Kashimura *et al.*, Solid State Commun. **93**, 675 (1995)

34. M. Tamura *et al.*, Solid State Commun. **93**, 585 (1995)

35. T. Miyazaki *et al.*, Phys. Rev. Lett. **74**, 5104 (1995); T. Miyazaki and K. Terakura; Phys. Rev. **B54**, 10452 (1996)

36. H. -P. Werner *et al.*, Slid State Commun. **65**, 809 (1988)

37. K. Yamaji; J. Phys. Soc. Jpn. **51**, 2787 (1982)

38. T. Mori *et al.*, J. Phys. Soc. Jpn. **56**, 3429 (1987)

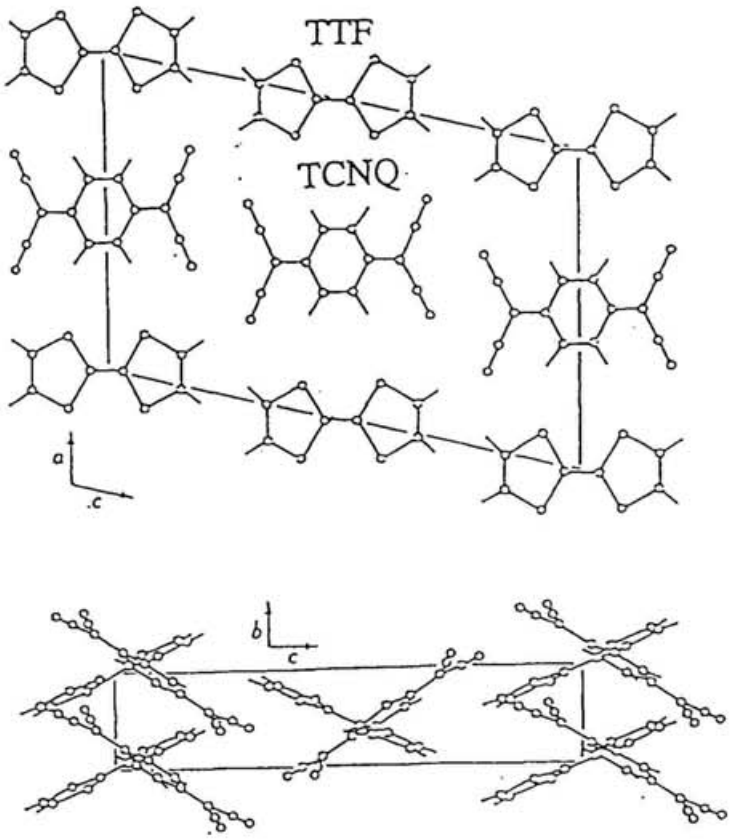

Fig. 1-1-1 Crystal structure of TTF-TCNQ.[2]

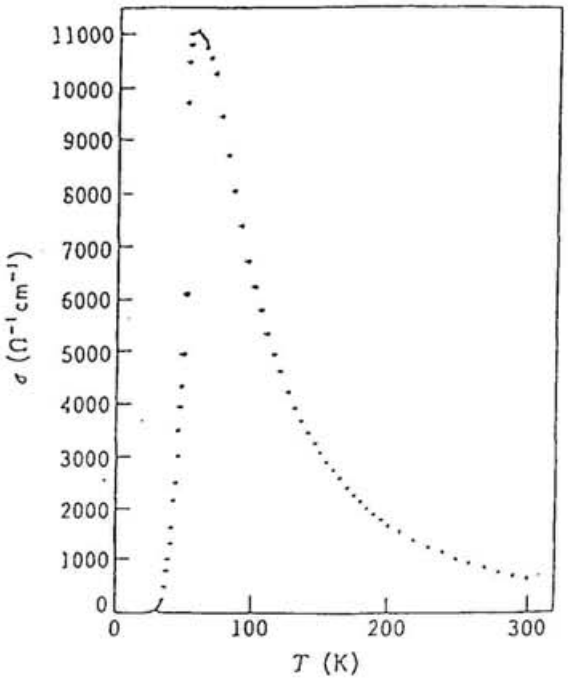

Fig. 1-1-2 Temperature dependence of resistivity, ρ, of TTF-TCNQ.[3]

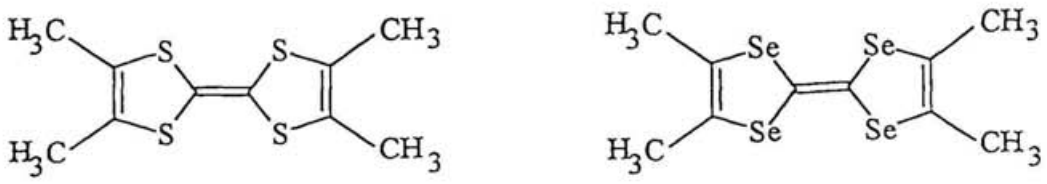

Fig. 1-1-3 TMTTF (left) and TMTSF (right) molecules.

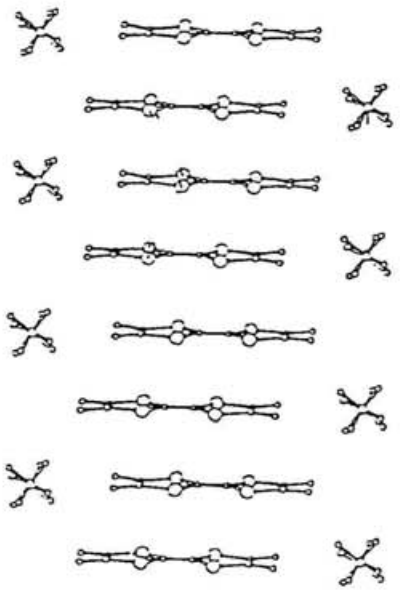

Fig. 1-1-4 Side view of the crystal structure of TM_2X.[6]

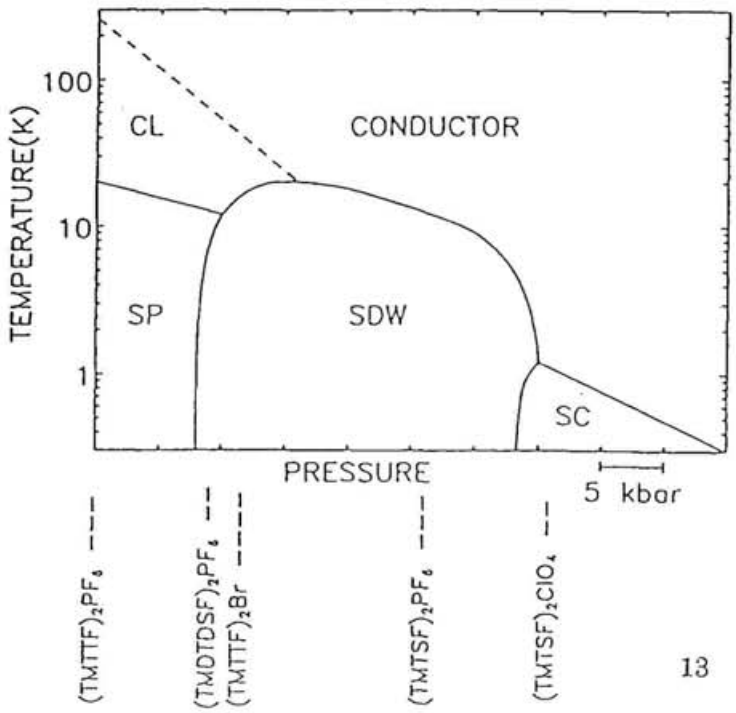

Fig. 1-1-5 General phase diagram for the TM_2X series. The dotted line marks means onset of charge localization. The position of each compound indicate their location at ambient pressure in this phase diagram [6].

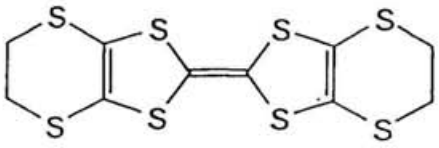

Fig. 1-1-6 BEDT-TTF molecule.

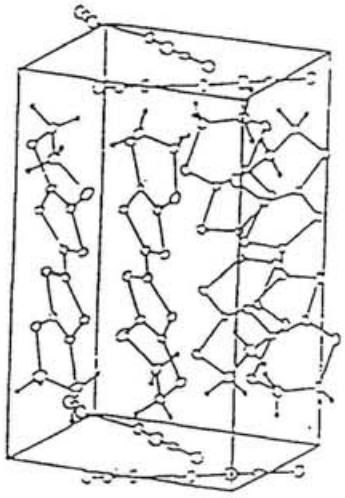

Fig. 1-1-7 Side view of crystal structure of $(BEDT\text{-}TTF)_2Cu(NCS)_2$.[12]

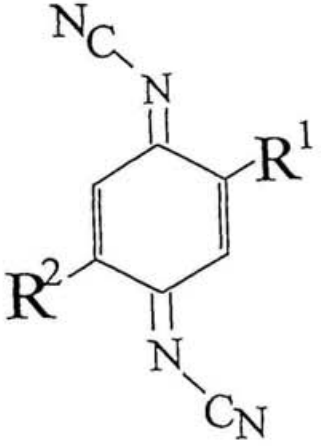

Fig. 1-2-1 R^1,R^2-DCNQI molecule. R^1/R^2 = CH_3 (Me), Br, I *etc.*

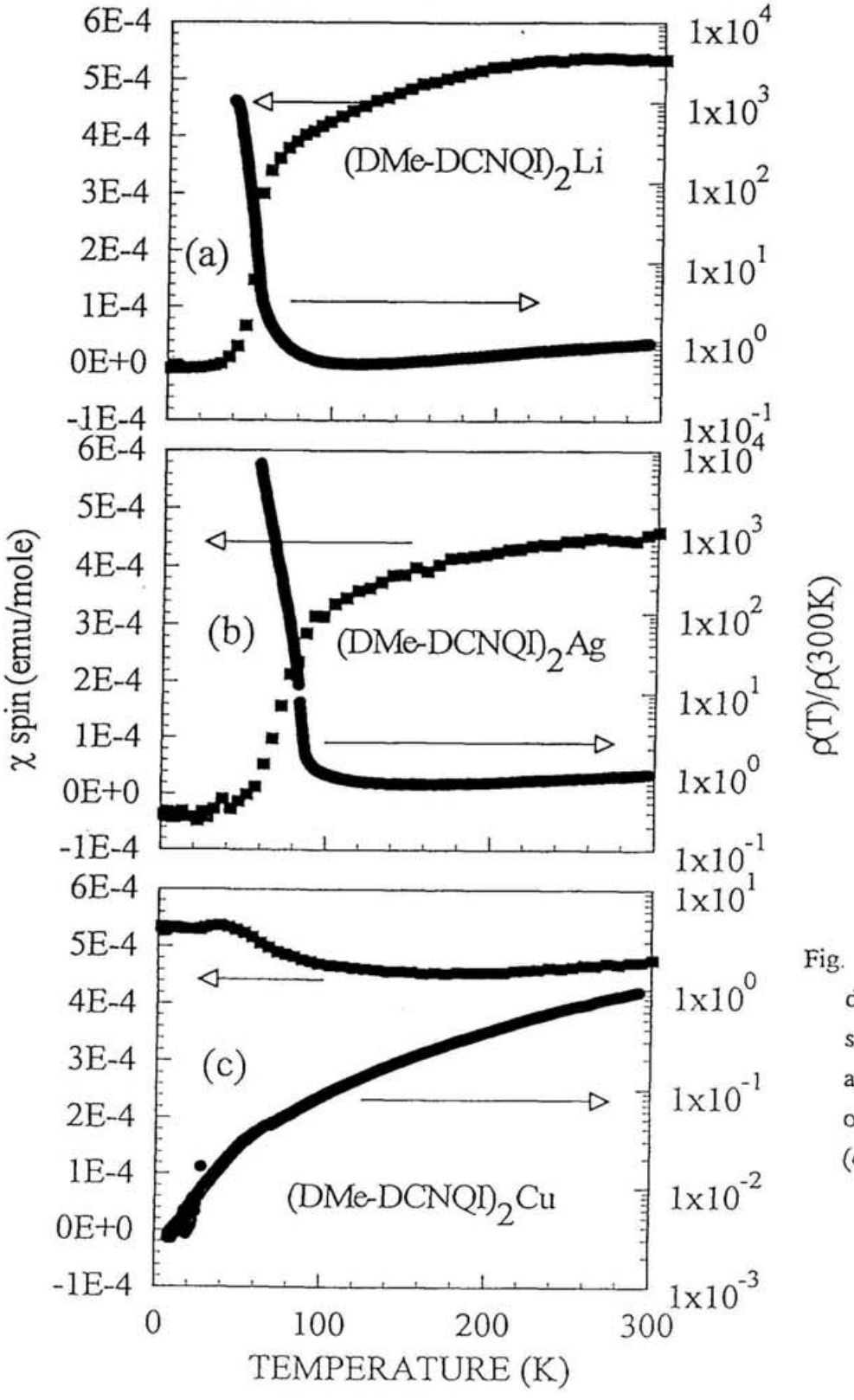

Fig. 1-2-2 Temperature dependence of spin susceptibility, χ_{spin} (left axis), and resistivity, ρ (right axis), of Li- (a), Ag- (b) and Cu-salts (c) with DMe-DCNQI.

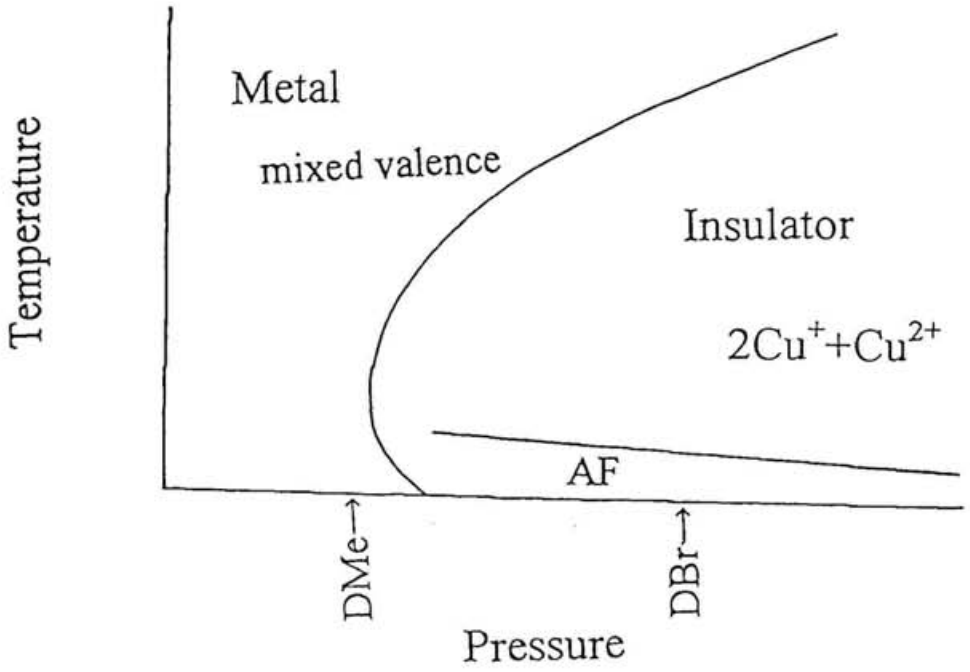

Fig. 1-2-3 General phase diagram of $(DCNQI)_2Cu$. The arrows their location at ambient pressure.

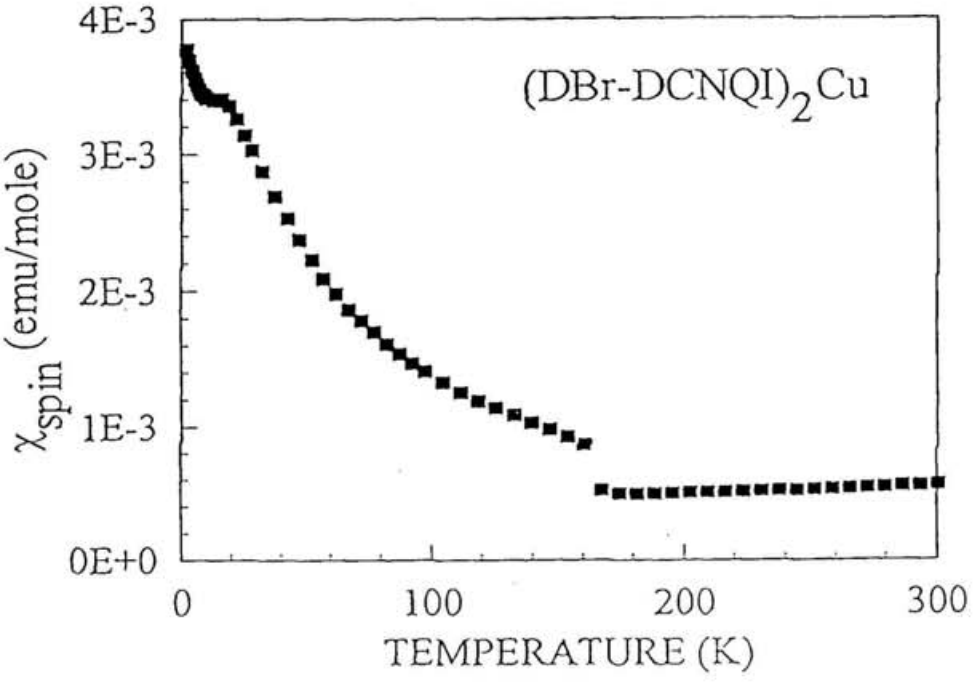

Fig. 1-2-4 Temperature dependence of χ_{spin} of $(DBr\text{-}DCNQI)_2Cu$. χ_{spin} follows a Curie-Weiβ law below the metal-insulator transition, and the system undergoes AF order at a lower temperature.

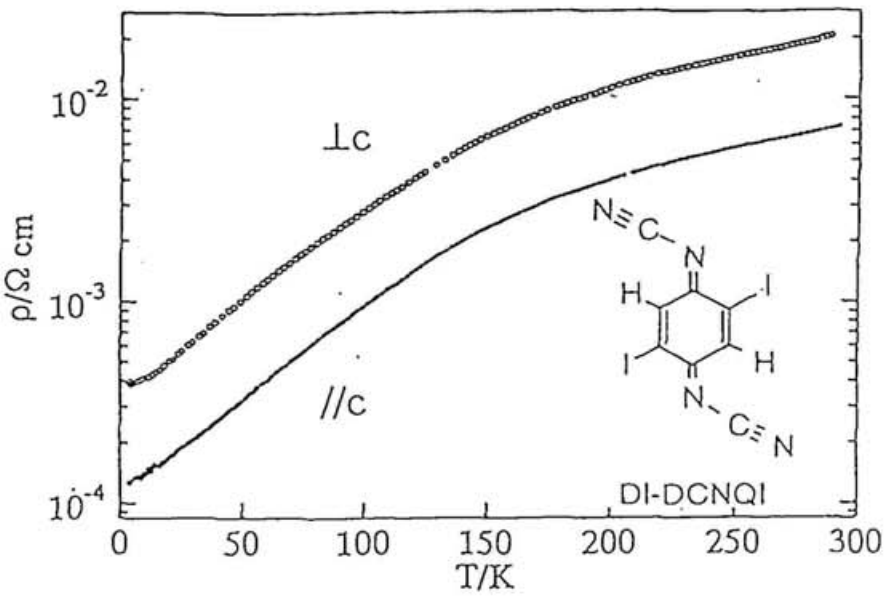

Fig. 1-2-5 Temperature dependence of resistivity parallel and perpendicular to the *c*-axis (stacking axis), $\rho_{\parallel}$ and $\rho_{\perp}$.[33]

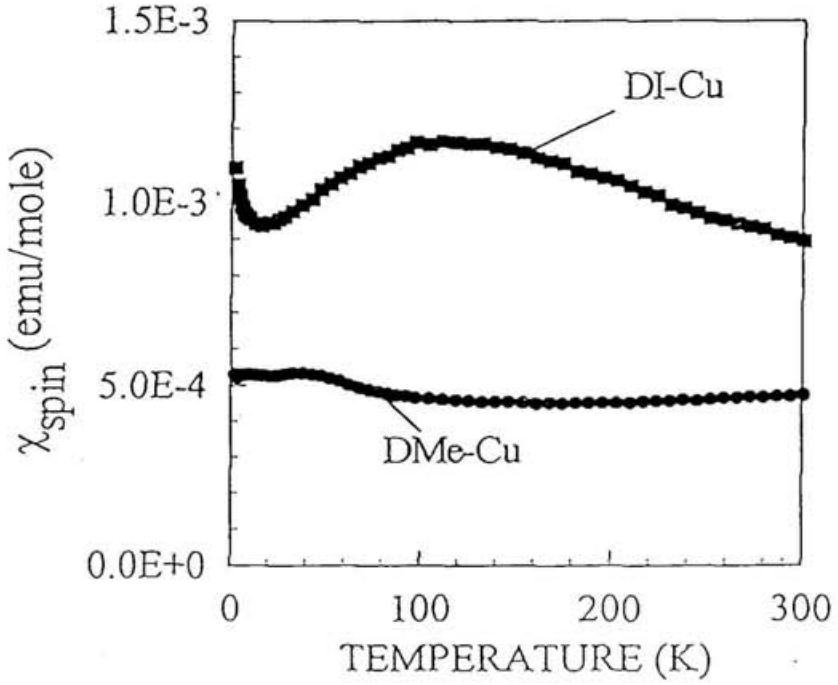

Fig. 1-2-6 Temperature dependence of χ_{spin} of DI-Cu. Isostructual DMe-Cu is also plotted for comparison.

Chapter 2.

NMR measurements

2-1 Principles

In this chapter, principles of the nuclear magnetic resonance (NMR) are introduced briefly.

Each nucleus interacts with its environment via hyperfine interaction[1,2]. There are three types of hyperfine interactions between 1) a nuclear spin and electron spins, 2) a nuclear spin and the orbital current of electrons and 3) a nuclear quadropole moment and field gradient.

The Hamiltonian of magnetic hyperfine interaction between the nuclear spin, I, at a site i and the electronic spin, S, at a site j may be express as

$$\hat{H} = g\gamma_I \hbar \vec{I}_i \cdot \hat{A}_{ij} \cdot \vec{S}_j , \tag{2-1}$$

where A_{ij} is a hyperfine coupling tensor. The diagonal term of the A_{ii}, which originates in the interaction between the nuclear spin and the electronic spin on the same atomic site, i, consists of such contributions as the Fermi contact (isotropic), dipole (traceless) and core polarization (isotropic) terms. The Fermi contact term originates from the direct contact of electrons of s-character with a nuclear spin. Note that the wave function of the electrons has a finite amplitude at the nuclear site. The core polarization term is caused by the imbalance of the up and down spins of s-shell at the nuclear position, which is induced by the exchange field of an unpaired and polarized electron spin in a non-s-orbital[3].

The total Hamiltonian for nuclear spins under a magnetic field, H_0, can generally be expressed as,

$$\hat{H} = \sum_i (-\gamma_I \hbar \vec{I}_i \cdot \vec{H}_0) + \sum_{i,j} g\gamma_I \hbar \vec{I}_i \cdot \hat{A}_{ij} \cdot \vec{S}_j + O + H_{eqQ} . \tag{2-2}$$

The first, second, third and fourth terms in eq. (2-2) originate in the interaction of nuclei with a static magnetic field (Zeeman interaction), electronic spins, orbital current and electric field gradient, respectively. The third term of eq. (2-2) is the contributions of Van Vleck paramagnetism and shielding diamagnetism giving chemical shift[4]. It is known that in the organic compound, the Van Vleck paramagnetism is quite small. Additionally, in the present work, the probed nucleus are ^{1}H and ^{13}C whose spin are 1/2 without quadropole moment. Therefore we do dot have to consider the fourth term. Apart from the chemical shift term, the eq. (2-2) can be reexpressed as

$$\hat{H} = \sum_i (-\gamma_I \hbar \vec{I}_i \cdot \vec{H}_{loc}), \tag{2-3}$$

with $\vec{H}_{loc} = \vec{H}_0 - \sum_i g A_{ij} \cdot \vec{S}_j$. The second term causes a shift of the resonance frequency from the condition, $\omega_N = \gamma_I H_0$ to an actual frequency, ω_{res}. The effect is called NMR shift, $K = (\omega_{res}-\omega_N)/\omega_N$. When the origin of the excess magnetic field is Pauli paramagnetism, K is called Knight Shift[5]. The relationship between NMR shift and spin susceptibility expressed as

$$K_i^{\alpha} = \sum_j A_{ij}^{\alpha} \chi_j^{\alpha}, \tag{2-4}$$

where α stands for the x, y and z axis, and χ_j is local spin susceptibility at the site j. Thus the measurements of NMR shift yield information on the local susceptibility. The hyperfine coupling tensor, A, can be determined from the slope of K-χ plot[6].

At thermal equilibrium, the population of the nuclear spins at the energy levels follow the Boltzmann distribution. As shown in Fig. 2-1-1a), there appears a net nuclear magnetization M_0 in this state. Absorption of radio frequency (rf) wave raises the nuclear spin temperature. When the upper and lower energy levels are equally occupied as shown

in Fig. 2-1-1b) , the net nuclear magnetization disappear (saturating state). Since the nuclear spin system interacts with thermal reservoir of the electrons through the hyperfine interaction, the nuclear magnetization will be recovered toward the value at the initial thermal equilibrium. The characteristic time of the recovery is called nuclear spin-lattice relaxation time, T_1. Since T_1 of a nuclear spin system depends on the state of the thermal reservoir, one can probe the physical properties of the reservoir system through the measurements of T_1. The time evolution of the nuclear magnetization after the saturation, M(τ), can be expressed as

$$M(\tau) = M_0(1 - e^{-\tau/T_1}) . \tag{2-4}$$

The relaxation rate, T_1^{-1} at a site i can be expressed in a general form of[8]

$$T_1^{-1} = 2\gamma_I k_B T A^2 \sum_{\vec{q}} \frac{\mathrm{Im}\,\chi_\perp(\vec{q},\omega)}{\omega_N} \tag{2-5}$$

where ω_N is the resonance frequency, and $\chi_\perp(q,\omega)$ is the dynamic susceptibility given by

$$\mathrm{Im}\,\chi(\vec{q},\omega) = \frac{\omega}{4k_B T}\int \langle \vec{S}_{\vec{q}}(t)\vec{S}_{-\vec{q}}(0)\rangle \cos\omega t dt . \tag{2-6}$$

T_1^{-1} probes the q-summation of the transverse dynamic susceptibility at a frequency of ω_N.

When the system is in a normal metallic state, eq. (2-5) becomes a well known form named Korringa relation[8],

$$T_1^{-1} = \frac{4\pi k_B T}{\hbar}\left(\frac{\gamma_I}{\gamma_e}\right)^2 K^2 . \tag{2-7}$$

In this case, since K is proportional to the density of states at Fermi level, $N(\varepsilon_F)$, T_1^{-1} is proportional to the square of $N(\varepsilon_F)$. If Pauli spin susceptibility is temperature-independent, T_1^{-1} is proportional to temperature.

In case of an antiferromagnet of local spins with the exchange interaction, J, the nuclear relaxation, which is dominated by the low frequency component of spin fluctuations of the exchange, can be expressed in the high temperature limit as[9]

$$T_1^{-1} = \sqrt{\frac{\pi}{2}} g^2 \gamma_I^2 A^2 \frac{S(S+1)}{3\omega_{ex}}, \tag{2-8}$$

where ω_{ex} is the exchange frequency of spins defined as

$$\omega_{ex}^2 = \frac{8zJ^2 S(S+1)}{3\hbar^2} \tag{2-9}$$

with z, the number of the nearest neighbor site. In the molecular approximation, J is related to the Nèel temperature, T_N, as

$$3k_B T_N = |J| zS(S+1). \tag{2-10}$$

The T_1^{-1} is proportional to J^1 and temperature-independent.

2-2 Measurement System

A standard pulsed NMR spectrometer was used in the present work. A block diagram is shown in Fig. 2-2-1. A powder or polycrystalline sample was packed into the glass tube of which the diameter is ~ 2.5 or 3.0 mm.

The NMR spectra were obtained by two different methods. One is Fast Fourier transformation of the quadrature-detected spin echo signals observed at a fixed frequency and field. This technique is available in case of relatively narrow spectrum compared with the inverse of the NMR pulse width. The typical $\pi/2$-pulse width in the study is 0.8 ~ 1.5 μsec for ^{1}H-NMR and 3.5 ~ 6 μsec for ^{13}C-NMR, which corresponds to ~ 300 kHz and ~

80 kHz, respectively. The other method is the measurement of the spin echo intensity as a function of frequency under a constant magnetic field. The frequency shift, K, relative to a standard material[10] was determined by the first moment of the spectrum. The line width is defined as the square root of the second moment of the spectrum. A relationship between the spectrum, shift and line width is shown schematically in Fig. 2-2-2.

The nuclear spin lattice relaxation time, T_1, was measured by the standard saturation recovery method. The saturated state was made by a set of $\pi/2$ pulses with an interval, t_i, in the condition, $T_2 \ll t_i \ll T_1$. The recovery curves of nuclear magnetization were obtained by plotting the spin echo intensity as a function of τ, a waiting time after the nuclear saturation. The typical pulse sequence and an example of the recovery curve are shown in Figs. 2-2-3a) and b), respectively.

References

1. V. Jaccarino; Proc. Int. School of Physics, Enrico Fermi, Course XXXVII (Academic Press, New York, 1967)
2. A. Abragam; Principles of Nuclear Magnetism, (Oxford University press, New York 1960)
3. R. E. Watson *et al.*, Hyperfine Interactions, ed. A. Freeman *et al.*, (Academic Press, 1967)
4. R. Kubo and Y. Ohta; J. Phys. Soc. Jpn. **11**, 547 (1956)
5. C. P. Slichter; Principles of Magnetic Resonance, 3rd ed. (Splinger-Verlag New York 1989)
6. A. M. Clogston *et al.*, Phys. Rev. **B121**, 1357 (1961)
7. T. Moriya; J. Phys. Soc. Jpn. **18**, 516 (1963)
8. J. Korringa; Physica **16**, 601 (1950)
9. T. Moriya; Prog. Theor. Phys. **16**, 23 (1956)
10. Correspond neutral DCNQI molecules are adopted as standard material.

Fig. 2-1-1

(a) A two level nuclear spin system under the thermal equilibrium. (b) The state of "saturation", in which no net nuclear magnetization exists.

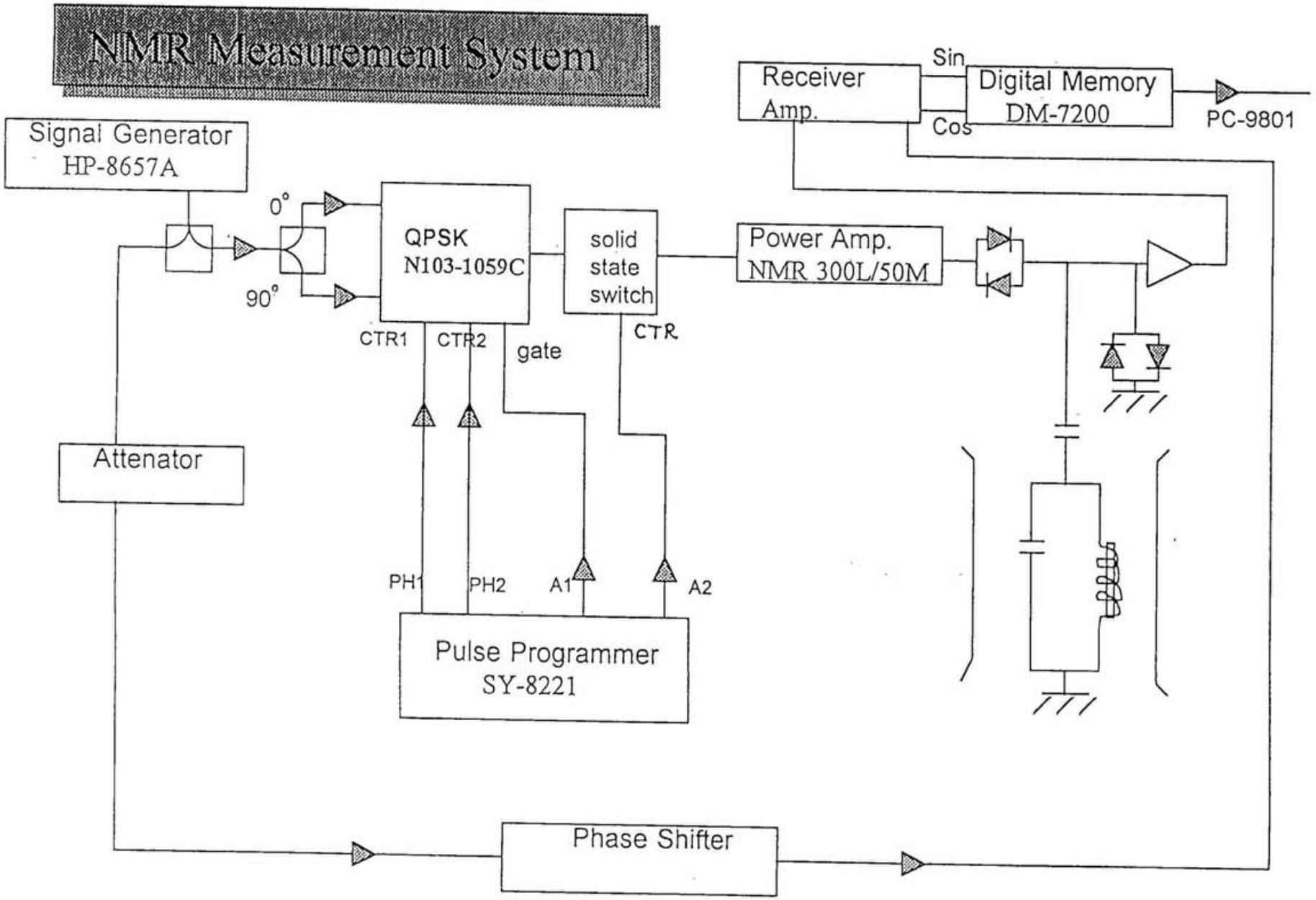

Fig. 2-2-1 Block diagram of the NMR measurement syste.

Components

- Magnetic field: superconducting solenoid type magnet: Oxford instruments, Maximum 90 kOe
- Signal Generator: Hewlett Packard 8657A
- Power Amplifier: ENI NMR 300L/500M and JEOL M3205 Maximum: 300 W
- Receiver Amplifier: THAMWAY unit type NMR receiver:

  rf Amp.: N141-5059A, 5-300 MHz

  Video Amp.: N144-1014A, DC-1 MHz

  ref. Phase shifter/phase sensitive detector:

  N072-1067A/N113-1067A, 25-50 MHz

  -1078A/ -1078A, 50-100 MHz

  -1089A/ -1089A, 100-200 MHz

  order made/order made, 200-400 MHz
- Phase cycling system: THAMWAY N103-1059C, 5-300 MHz
- Pulse Generator: IWATSU SY-8221
- Digital Memory: IWATSU DM7200
- Temperature controller: CONDUCTUS TLC-20

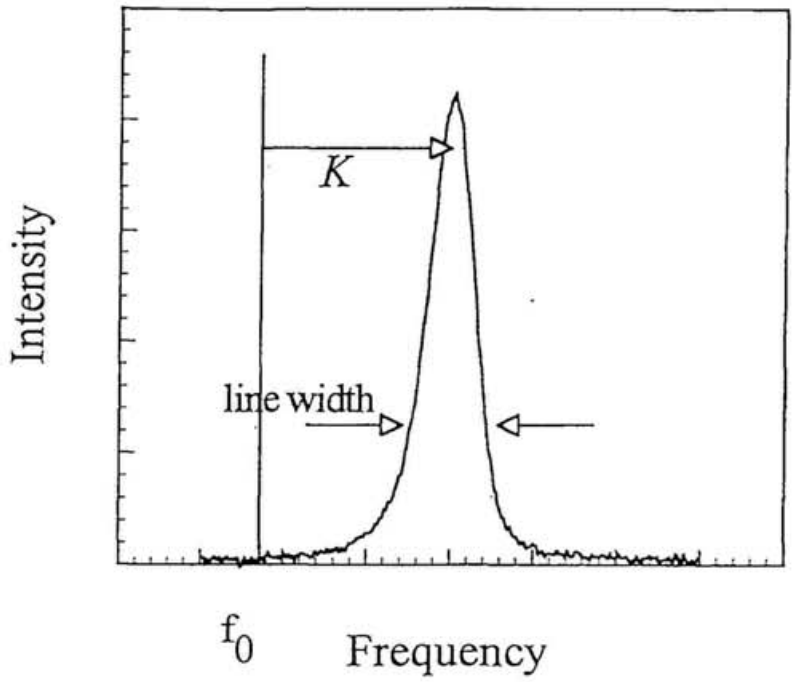

Fig. 2-2-2 A relationship between the spectrum, shift, K, and line width.

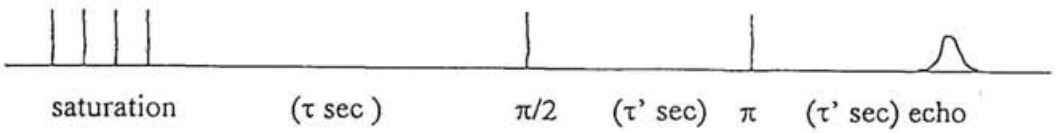

Fig. 2-2-3a) The typical pulse sequence.

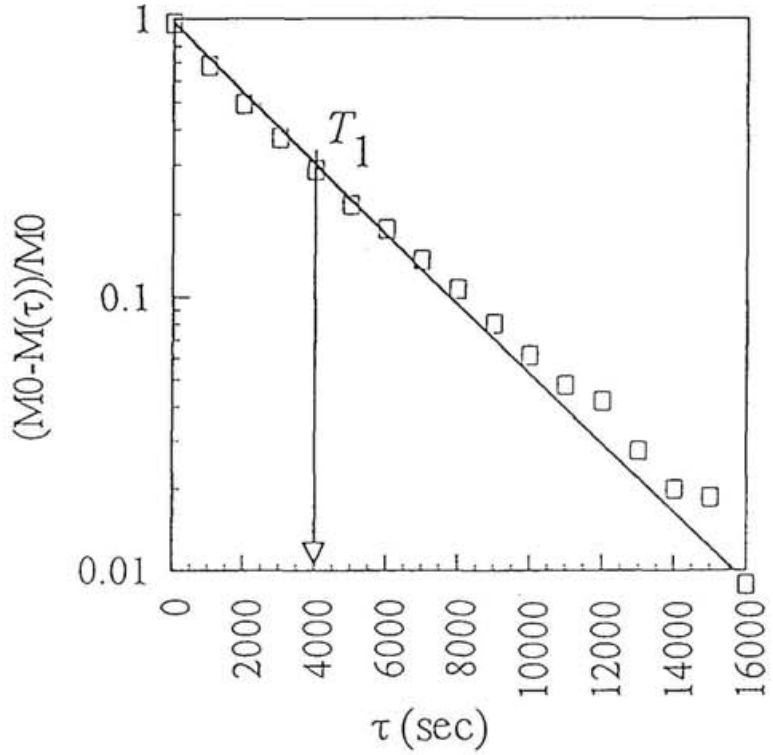

Fig. 2-2-3b) Example of the recovery curve.

Chapter 3.

Electronic States of DI-DCNQI Metal Complexes

3-1 Introduction

In this chapter, investigations of the electronic states constructed by DI-DCNQI 1D columns are described. As mentioned in chapter 1, it is suggested from the measurements of ρ and χ that the DI-system is more 3D and highly correlated than the DMe-system. The band structure calculations also predict a narrower 1D π band in DI-DCNQI column. This feature may be involved in the manifestation of electron correlation in DI-Cu. There are arguments on the origin of the electron correlation; 1D π band or Cu 3d band? In this sense, the 1D electronic state in DI-DCNQI stack itself should be characterized. The Li/Ag salt, DI-Li/DI-Ag, is expected to afford a nearly pure π electronic system without hybridization with 3d orbital. DI-Li and DI-Ag have been newly synthesized in the present study. In chapter 3-2, the preparation and characterization of the samples are described. The conducting and magnetic properties of DI-Ag and DI-Li are discussed in chapter 3-3. Further investigations of DI-Ag by ^{13}C-NMR are presented in chapter 3-4. The ground state of DI-Ag is uncovered in chapter 3-5. In chapter 3-6, the NMR characterization of DI-Li is described. In chapter 3-7, DI-Cu is investigated by NMR measurements at selective nuclear sites and is discussed from the viewpoint of hybridization between the DI-DCNQI 1D π orbital and the Cu 3d orbital. A summary is given in chapter 3-8.

3-2 Sample preparation

The crystals of DMe-Ag and DI-M were prepared by the electrochemical reduction; a constant current of 1μA was applied for about one week to the acetonitril (CH_3CN) solution containing DMe-DCNQI or DI-DCNQI and $LiBF_4$ for Li salt, $AgBF_4$ for Ag salt and $[Cu(CH_3CN)_4]ClO_4$ for Cu salt[1]. Needle like crystals were obtained.

The structure of the new compounds, DI-Ag and DI-Li, was found to be tetragonal like other DCNQI-M systems such as DMe-M and DI-Cu by single-crystal *X*-ray analysis. The lattice constants at room temperature are summarized in Table 1.

Table 3.1 Lattice parameters of DCNQI-M complexes.

Material	*a*(Å)	*c*(Å)	*V*(Å^3)
DI-Cu [2]	21.721	4.096	1932.7
DI-Ag	22.378	4.055	2030.6
DI-Li [3]	21.995	4.076	1971.7
DMe-Cu [4]	21.548	3.871	1797.4

3-3 Conducting and magnetic properties of (DI-DCNQI)$_2$M [M = Ag, Li]

Figures 3-3-1 and 3-3-2 show the temperature dependence of the *c* axis resistivity normalized to the room temperature value and magnetic susceptibility for DI-Ag/Li. The data of other isostructual salts, which reproduced the earlier results[5-8], are also plotted for comparison. In Fig. 3-3-2, the diamagnetic core contribution is corrected according to the Pascal' law; -9.15×10^{-5}, -1.402×10^{-4}, -0.6×10^{-5}, -1.2×10^{-5} and -2.4×10^{-5}

emu/mole for DMe-DCNQI, DI-DCNQI, Li^+, Cu^+ and Ag^+, respectively.

The paramagnetic nature of DI-Ag/Li shown in Fig. 3-3-2 evidences that this compound is not a band insulator. The temperature dependence of χ of DI-Ag/Li is of the Curie-Weiβ type at higher temperatures but forms a broad peak around 35 K for DI-Ag and a shoulder around 30 K for DI-Li reminiscent of the so-called Bonner-Fisher type[9]. This behavior implies low dimensionality in the spin systems although the decrease of χ at lower temperatures is not so prominent as the Bonner-Fisher behavior, that may be an effect of 3D interchain coupling. The parameters obtained by fitting of the data above 200 K to the Curie-Weiβ type curve are summarized in Table 3-2.

Table 3-2. Parameters obtained by the Curie-Weib fitting of χ above 200 K. C, θ and A are the Curie constant, the Weiβ temperature and the spin fraction per formula unit.

Material	C (emu K/mole)	θ (K)	A(%)
DI-Ag	0.32	-71	87
DI-Li	0.30	-49	80

For DI-Ag, χ shows a kink around 10 K, which is considered as a sign of magnetic order. This is quite different from the nonmagnetic state in DMe-Ag/Li, which shows a vanishing spin susceptibility below the (spin-) Peierls transition. Such a kink-like structure is apparent in DI-Li as well. However, it is indistinguishable from a steep increase of

possible Curie term. It is interesting to note that DI-M and DMe-M have respective values of χ irrespectively of M at higher temperatures although there occur various low temperature ground states.

As seen in Fig. 3-3-1, DMe-Li/Ag and DI-Ag show nonmetallic ground states while DMe-Cu and DI-Cu are metallic in the whole temperature range. For DI-Ag, ρ increases without any anomaly below room temperature, that is a contrast to the abrupt increase of ρ at 60 K for DMe-Li and 80 K for DMe-Ag due to the (spin-)Peierls transition. This indicates that a charge excitation gap opens even at room temperature for DI-Ag. An activation plot of ρ versus inverse T shown in Fig. 3-3-3 gives a charge gap of 490 K for DI-Ag. As for ρ of DI-Li, our preliminary result is indicative of the nonmetallic behavior like DI-Ag, as shown in Fig. 3-3-1. However, its reproducibility has not yet been guaranteed at present. So, we do not enter into the detailed analysis of the ρ of DI-Li.

3-4 Nature of Insulating State of (DI-DCNQI)$_2$Ag; ^{13}C-NMR study

The DI-Ag is expected to have the electronic system with a nearly pure π electron band as mentioned earlier. If the molecular stacking is uniform, the filling of 1D π electronic band is expected to be a quarter, giving a metallic state in the uncorrelated case. In fact, DMe-Ag behaves metallic at a higher temperature region. The resistivity of DI-Ag show an insulating behavior in the whole temperature range below room temperature and the χ shows no spin gap. The magnetism is typical of a Mott insulator.

To obtain further information on the origin of the insulating nature of the DI-Ag, ^{13}C-NMR measurements have been performed at the cyano site in the DI-DCNQI molecule which has large hyperfine coupling with electrons.

The measurements were made for a polycrystalline sample (~20mg) in a temperature range between 1.7 K and 280 K. The NMR frequency was 87.6MHz, which corresponds to an external field of 8.2 Tesla. The ^{13}C-NMR spectra were obtained by the fast Fourier transformation (FFT) of the spin echo signal following the $\pi/2$-π pulse sequence in the higher temperature region. The width of $\pi/2$-pulse was about 4μsec corresponding to the spectral width of ~120kHz. Therefore the FFT method was not available at lower temperatures, where the spectrum became broader than the inverse of the pulse width. In such a case, the spectra were constructed in terms of the echo intensity measured as a function of frequency.

^{13}C-NMR spectra are shown in Fig. 3-4-1(a), (b) and (c) (Note the different scales of the transverse axes.) At higher temperatures above 200 K, ^{13}C-NMR spectra are single lines, which is consistent with the fact that all of the ^{13}C sites are crystallographically equivalent. Below 200 K, however, the spectra get split into two lines with different shift, K, and width, Δ. The narrower line with the smaller shift and the broader one with the larger shift are called inner line and outer one hereafter. Although the outer line is much broader than the inner line, the intensity of both lines are comparable. Therefore, the line splitting indicates separation of the carbon sites into two different electronic circumstances with equal populations. The K and Δ of the NMR line of a powdered sample are expressed as[10],

$K \propto \vec{I}\hat{A}\vec{S}$ and $\Delta \propto < (\vec{I}\hat{B}\vec{S})^2 >^{1/2}$

using the isotropic and anisotropic terms of the hyperfine coupling tensor, $\hat{A}$ and $\hat{B}$; trace $[\hat{A}] \neq 0$ and trace $[\hat{B}] = 0$. The $<(IBS)^2>$ stands for the powder average. As K is proportional to the local electron density of LUMO around the ^{13}C site, the line splitting in the paramagnetic state is considered to indicate charge ordering into two sublattices. This is a charge modulation type of $4k_F$ CDW with two fold periodicity along the c axis and is reminiscent of the Wigner crystal; DI-DCNQI molecules with rich and poor electron densities are arranged alternately along the c axis. This type of CDW is contrast to the lattice modulation type, which is widely observed in many organic systems with quarter filling band. This situation is depicted in Fig. 3-4-2. The outer/inner line comes from the nuclei on the DI-DCNQI molecules with rich/poor population of electron. The NMR shifts of the inner and outer lines, denoted by Ki and Ko, are plotted as a function of temperature in Fig. 3-4-3. The Ki/(Ki+Ko) and Ko/(Ki+Ko), which measures relative populations of electron in the respective molecules, are sown in Fig. 3-4-4. The charge imbalance starting around 220 K saturates to ~ 3:1 below 150 K. This charge ordering with $4k_F$ CDW modulation is concluded to be responsible for the nonmetallic state of DI-Ag.

As shown in Fig. 3-4-1(b) and (c), the outer line becomes remarkably broadened and finally spread out with temperature decreased, while the inner line, although broadening is appreciable, remains observable down to the lowest temperature available. As suggested by the susceptibility and evidenced by the ^{1}H-NMR, which will be described below, thhe ground state is antiferromagnetically ordered state. In this context, the broadening of the line is reasonably attributed to the fluctuations of $2k_F$ AF ordering in the $4k_F$ charge

ordered state. The "*K*o" site experiences serious fluctuations of local field, which makes the broadening prominent. On the other hand, at the "*K*i" site situated in between the "*K*o" site, the local field due to the AF short range order should be canceled, that explains why the inner line alone is free from spreading out.

3-5 Ground state of (DI-DCNQI)$_2$Ag; ^{1}H-NMR study

The ^{13}C site has strong hyperfine coupling with LUMO electrons so that ^{13}C-NMR was useful to probe the electronic structure in the paramagnetic state, as seen in the previous chapter. By this reason, however, the ^{13}C-NMR becomes spread out when the magnetic ordering is approached. In this situation, ^{1}H site, which has much smaller hyperfine coupling constant, plays a complimentary role. In order to clarify the ground state of DI-Ag ^{1}H-NMR experiments were performed. The ^{1}H is connected directly to the six-membered ring of the DI-DCNQI molecule. The measurements were performed for the same sample as used in the ^{13}C-NMR measurements. The NMR frequency was 85.3 MHz, which corresponds to 2.0 tesla. The ^{1}H-NMR spectra are shown in Fig. 3-5-1(a). Below about 200 K, the line shape becomes asymmetric. This reflects the shift inhomogeneity due to the freezing of the $4k_F$ CDW or charge ordering. The spectra were not separated so clearly as in ^{13}C-NMR. This is because the hyperfine coupling between ^{1}H nuclei and LUMO electrons are very small and the nuclear dipolar broadening is convoluted on the two lines. A drastic change occurs at 5.5 K. Above this temperature, the line width is an order of ten kHz, while, at lower temperatures, the spectra suddenly get broadened over several hundreds kHz around the origin of the shift; a spectrum at 1.7 K is shown in Fig.

3-5-1(b). The broadened spectra are obtained by the frequency sweep of the spin echo intensity over a range of ± 800 kHz because the spectra spread out of the frequency width attained by the present rf pulse width. This broadening indicates generation of inhomogeneous local field and is a microscopic evidence of magnetic transition. Since χ above and below the transition has similar magnitudes as seen in Fig. 3-3-2, it cannot be ferromagnetic. Therefore, it is concluded that the nature of the magnetic transition is AF. The temperature dependence of the line width in Fig. 3-5-2 shows clearly that the transition temperature is 5.5 K.

Figure 3-5-2 also shows T_1^{-1} as a function of temperature. At 5.5 K, where the spectra starts to be broadened, T_1^{-1} forms a peak. This is an additional evidence of an AF transition. The gradual increase of T_1^{-1} toward 5.5 K from 10 K is a manifestation of the critical slowing down of the spin fluctuations and a rapid decrease below that reflects fluctuations in the staggered magnetization[11].

The ground state of DMe-Ag is viewed as Peierls state driven by Fermi surface nesting or spin-Peierls state. [In the intermediate temperature range from 100 K down to 80 K, the resistivity of DMe-Ag tends to increase. The nonmetallic behavior in this temperature range can be explained in two ways; one is in terms of pseudo gap due to the $2k_F$ CDW fluctuations, which condense below 80 K, and the other is a Mott like insulator due to $4k_F$ CDW with tendency of spin and charge localization. The former interpretation leads to a picture of Peierls ground state while the latter to a picture of spin-Peierls ground state. These two pictures are difficult to distinguish.] On the other hand, DI-Ag is an AF insulator. The difference of the ground states is understood in terms of the difference of the band width and the dimensionality in the electronic system as follows. According to

the first principle band calculations, the interchain and intrachain hopping integrals, $t_\perp$ and $t_\parallel$, for DI-system are about three times larger and one half smaller than for DMe-systems, respectively, indicating that the DI-system has a narrower band width and is more 3D than the DMe-system. The former aspect in DI-Ag enhances the effect of the electron correlation and drives the system into the insulator in the whole temperature range. The latter aspect is responsible for AF ground state of this material because an Néel state is stabilized with increasing interchain interaction[12] in quasi 1D electronic system. The difference of dimensionality also explains the fact that DI-Ag has larger spin susceptibility than the DMe-Ag because the χ inversely correlates with $t_\parallel$ through density of states in the metallic regime or through the exchange interaction, J, in the paramagnetic insulating regime.

This system is highly correlated π electronic system having $4k_F$ CDW without $2k_F$ CDW. At low temperature, DI-Ag undergoes as AF transition. The insulating state of this compound is qualitatively different from those of other isostructual DCNQI-M complexes studied so far; the nonmagnetic (spin-) Peierls ground state in DMe-Ag/Li[13] and the cooperative Peierls and Mott insulating state in DMe-Cu under pressure[14]. The DI-Ag is unique among DCNQI-M complexes in that the π electrons are responsible for magnetic ordering. The magnetism revealed here indicates nature of the Mott insulator and demonstrates importance of electron correlation in the π-electron system in DCNQI-M complexes.

3-6 Comparison between (DI-DCNQI)$_2$Ag and (DI-DCNQI)$_2$Li

In this chapter, the electronic properties of DI-Li are discussed by comparing the ^{1}H-NMR characteristics of the DI-Li and DI-Ag. The preparation of ^{13}C enriched DI-Li sample is not yet successful.

Although it was difficult to obtain the high quality crystal of DI-Li, fortunately, samples with considerablely diminished Curie term are synthesized after many trials. ^{1}H-NMR measurements were performed at 200 MHz (4.7 tesla) for both systems.

^{1}H-NMR spectra at 200 MHz of DI-Li and DI-Ag are shown in Fig. 3-6-1a) and b). In a higher temperature region, the spectra of both salts are symmetric single lines. In the lower temperature region, $T < 100$ K for DI-Li and $T < 200$ K for DI-Ag, the spectra became asymmetric. The typical ^{1}H-NMR spectra of DI-Li below 100 K and of DI-Ag below 200 K are shown in Fig. 3-6-2a) and b), respectively. The spectra can be reproduced by a sum of two Gaussian, as shown in the figures. Although the significant line separation has not been observed due to the small hyperfine coupling between ^{1}H and LUMO of the systems, the essential feature of the spectra are shared by ^{1}H and ^{13}C-NMR spectra of DI-Ag. This is a manifestation of the $4k_F$ CDW as mentioned in chapter 3-4.

Temperature dependence of ^{1}H-NMR linewidth and the relaxation rate, T_1^{-1},of both salts are shown in Figs. 3-6-3, and 3-6-4. The line width of DI-Li increases steeply below 20 K like DI-Ag and is attributable to AF fluctuations. The peak formation of T_1^{-1} is not so clears as the case of DI-Ag but seems to occur around ~3 K. At higher temperatures, the difference between T_1^{-1} of the two systems becomes apparent, suggesting the difference of the electronic states. However, the two systems are considered to have the

common nature of the insulating state and the ground state.

3-7 Electronic state of (DI-DCNQI)$_2$Cu; an electronic system with π-d hybridization

It is known that when Ag/Li is replaced by Cu, the d orbital in Cu are hybridized with π orbital in DCNQI at least for the DMe-system. We can imagine the same situation in the DI-system. The NMR measurements at the selective nuclear sites in the DI-Cu, ^{1}H and ^{13}C at cyano site, were performed. The ^{1}H- and ^{13}C-NMR spectra are shown in Figs. 3-7-1 and 3-7-2, respectively. The spectra at both nuclear sites are constructed by single line. In Fig. 3-7-3, the spectral shifts of ^{13}C- and ^{1}H-NMR, ^{13}K and ^1K, from the line position of neutral DI-DCNQI molecule are shown in comparison with χ. Both of ^{13}K and ^1K form broad peaks like that of χ. However, it should be noted that the peak temperature of ^1K is lower than that of χ while the peak temperature of ^{13}K is slightly higher than that. The overall temperature dependence of χ is in between the two profiles. Since K probes the local spin susceptibility, this fact is considered as a microscopic evidence that the electronic structure consists of several bands with different characters, which is believed to come from hybridization of the π and d orbitals; ^{1}H-NMR detects the electrons of π-band preferentially, while ^{13}C-NMR at the cyano group coordinated to the Cu ions can probe the d-electrons through the off-site core polarization as well as the π electrons.

The Cu salts are considered to be conductors doped into the (spin-)Peierls insulator

(DMe-Ag/Li) and Mott insulator (DI-Ag/Li) in a sense that hybridization modifies the band structure and controls band filling of the π band at the same time. It is interesting to note that χ at higher temperatures is almost determined by the kind of DCNQI molecule irrespectively of the metal ions, Cu or Ag/Li. This has an implication of a dominant role of the π electronic system in magnetism even for the Cu salts.

3-8 Summary

The electronic states of metal (Li, Ag and Cu) complexes of DI-DCNQI were investigated by ρ, χ, ^{1}H- and ^{13}C-NMR measurements. The newly synthesized DI-Ag and DI-Li are insulators below room temperature. The $4k_F$ CDW has been observed from line separation of the ^{13}C-NMR spectra of DI-Ag. ^{1}H-NMR also detected the $4k_F$ CDW in the DI-Ag/Li. It is emphasized that the CDW in DI-Ag/Li is the charge ordering rather than the lattice modulation type. The DI-Ag/Li is understood as Mott insulator by the large Coulomb repulsion. The ground state of DI-Ag/Li is AF. The AF interaction, J of DI-Li is little smaller than that of DI-Ag. DI-Ag/Li, which is considered as a nearly pure π electronic system like DMe-Ag/Li, is the first case of π electron antiferromagnet among DCNQI-M systems. It has been observed that there were not significant AF order in the DI-Li.

The difference of the electronic states between the Ag/Li salts of DMe-DCNQI and DI-DCNQI is explained by the difference of the band width and the dimensionality of the electronic states. In fact, according to the estimation of the transfer integral by the band calculation, the DI-system is more three dimensional and has a narrow band than the

DMe-system. In DI-systems, the effect of electron correlation is enhanced.

The NMR spectra at ^{1}H and cyano ^{13}C sites in DI-Cu were measured. Both of the shift, ^{1}K and ^{13}K, form broad peaks like χ. However, they showed different temperature dependence. The overall temperature dependence of χ is in between the two profiles of the shift. ^{13}C-NMR at the cyano group coordinated to the Cu ions can probe the d orbital through the off-site core polarization as well as the π band. This is the evidence of the existence of the hybridization between the Cu 3d orbital and 1D π band even in the DI-system.

The ground state of DI-Ag is a magnetic insulator, while the isostructual DI-Cu is a paramagnetic metal with hybridization of the π orbitals with Cu 3d orbitals. The present result of DI-Ag shows an important role of π band in electron correlation manifesting itself in ,e.g. enhancement of spin susceptibility in the DI systems.

References

1. R. Kato *et al.*, Chem. Lett. **1987**, 5913 (1987)
2. Y. Kashimura *et al.*, Solid State Commun. **93**, 675 (1995)
3. H. Sawa; private communications
4. R. Kato *et al.*, J. Am. Chem. Soc. **111**, 5224 (1989)
5. A. Aumüller *et al.*, Angew. Chem. Int. Ed. Engel. **25**, 740 (1986)
6. H. J. Gross *et al.*, J. Phys. France **50**, 2347 (1989)
7. P. Erk *et al.*, Adv. Matter **3**, 311 (1991)
8. H. -P. Werner et al., Slid State Commun. **65**, 809 (1988)
9. J. C. Bonner and M. E. Fisher; Phys. Rev. **135**, A640 (1964)
10. C. P. Slichter; Principles of Magnetic Resonance, (third ed. Splinger-Verlag, New York, 1989)
11. T. Moriya and K. Ueda; Solid State Commun. **15**, 169 (1974)
12. S. Inagaki and H. Fukuyama; J. Phys. Soc. Jpn. **52**, 3620 (1983)
13. R. Moret *et al.*, J. Phys. France **49**, 1925 (1988); M. Meneghetti *et al.*, Synth. Met. **41-43**, 1775 (1991)
14. K. Hiraki *et al.*, J. Phys. Soc. Jpn. **64**, 2203 (1995); T. Takahashi *et al.*, Synth. Met. 55-57, 2281 (1993)

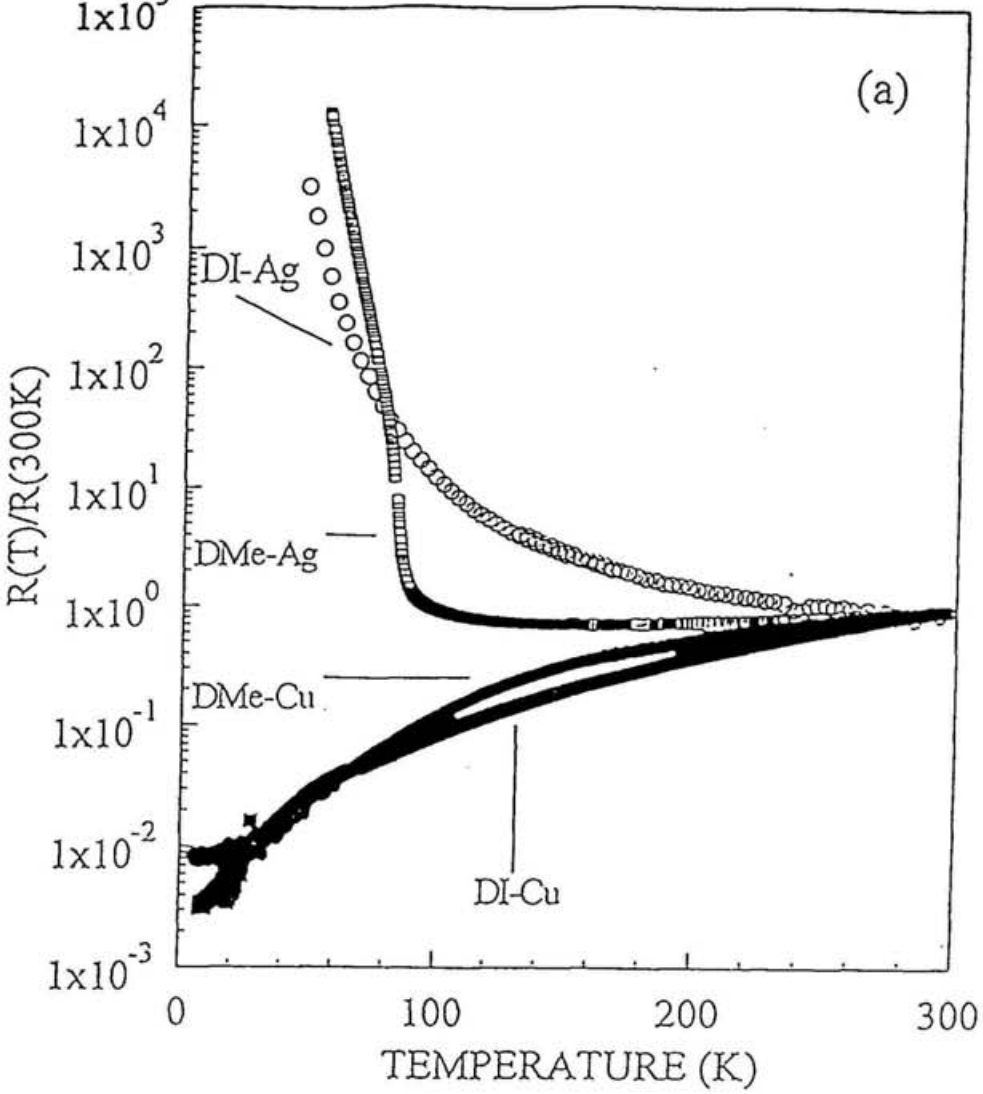

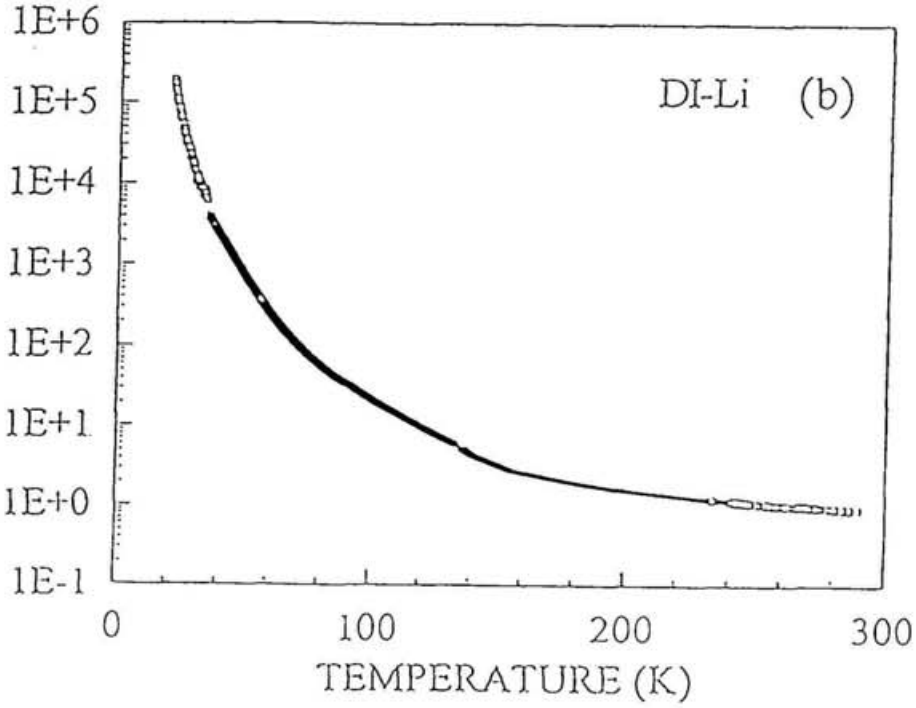

Fig. 3-3-1 Temperature dependence of the *c*-axis resistivity normalized to the room temperature value of DI-Ag (a) and DI-Li (b).

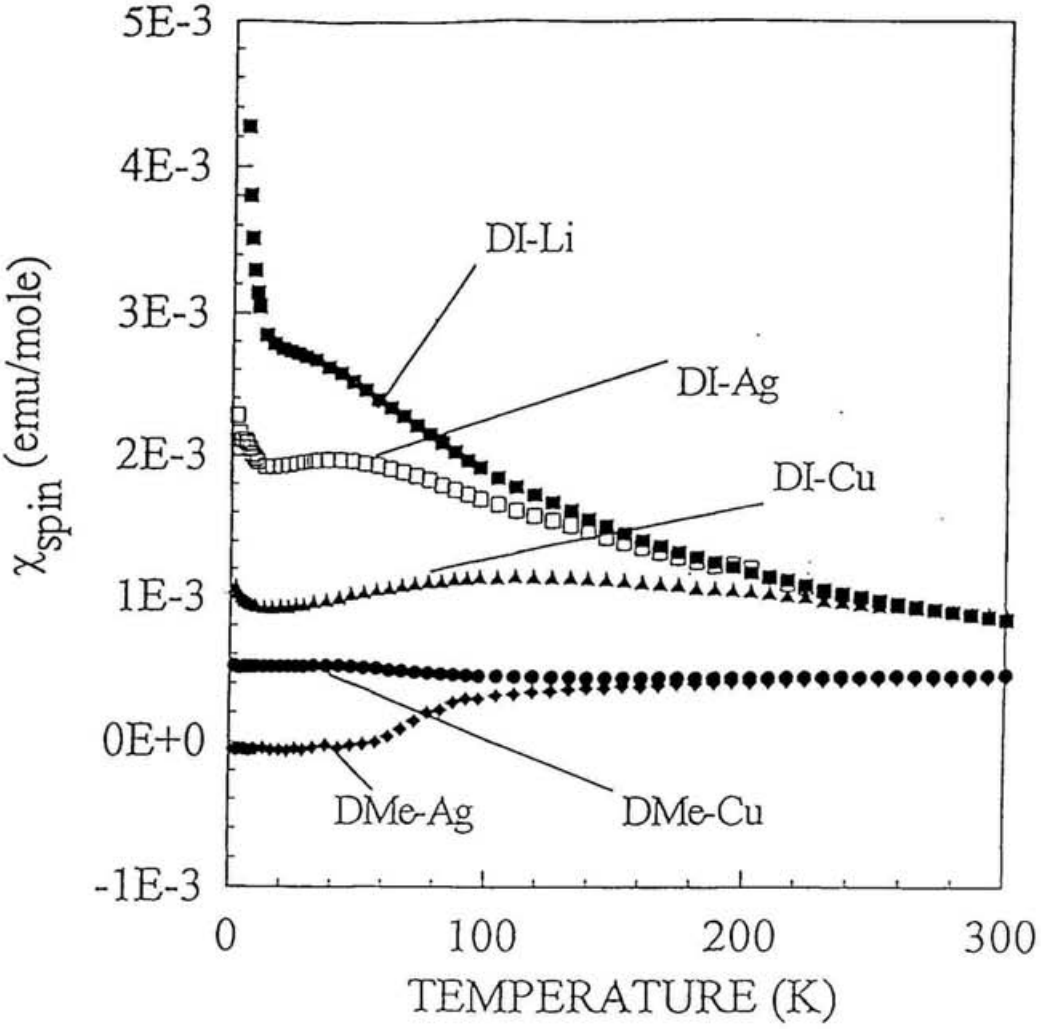

Fig. 3-3-2 Temperature dependence of spin susceptibility.

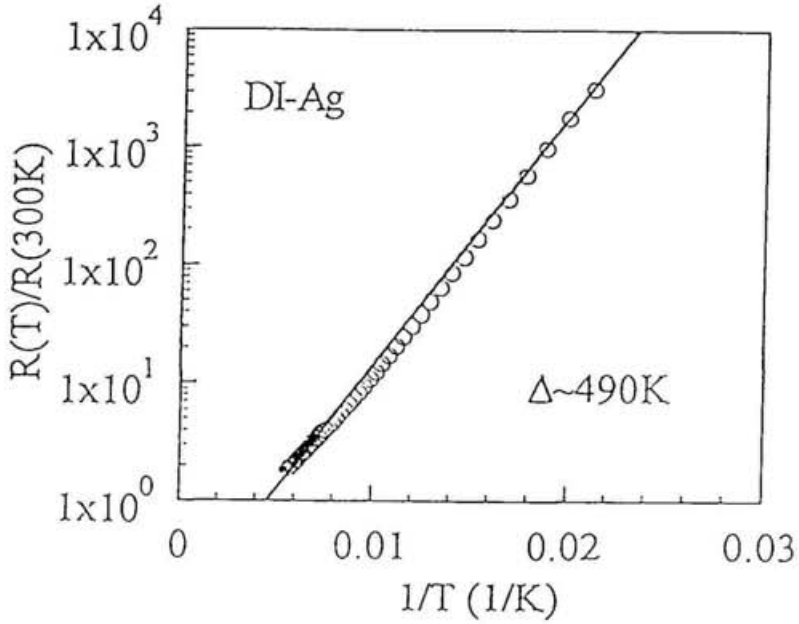

Fig. 3-3-3 Activation plot of resistivity.

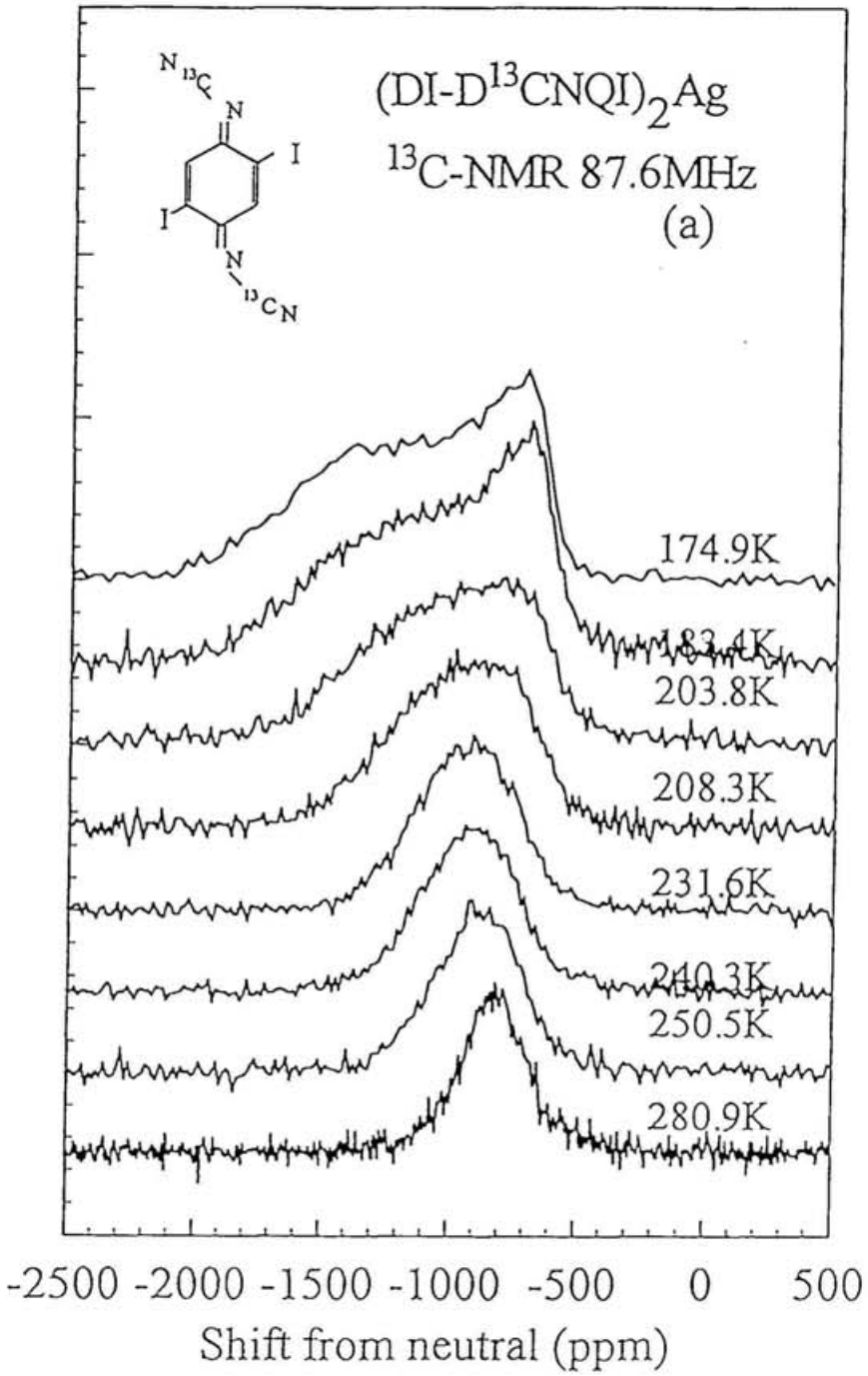

Fig. 3-4-1 ^{13}C-NMR spectra of DI-Ag.

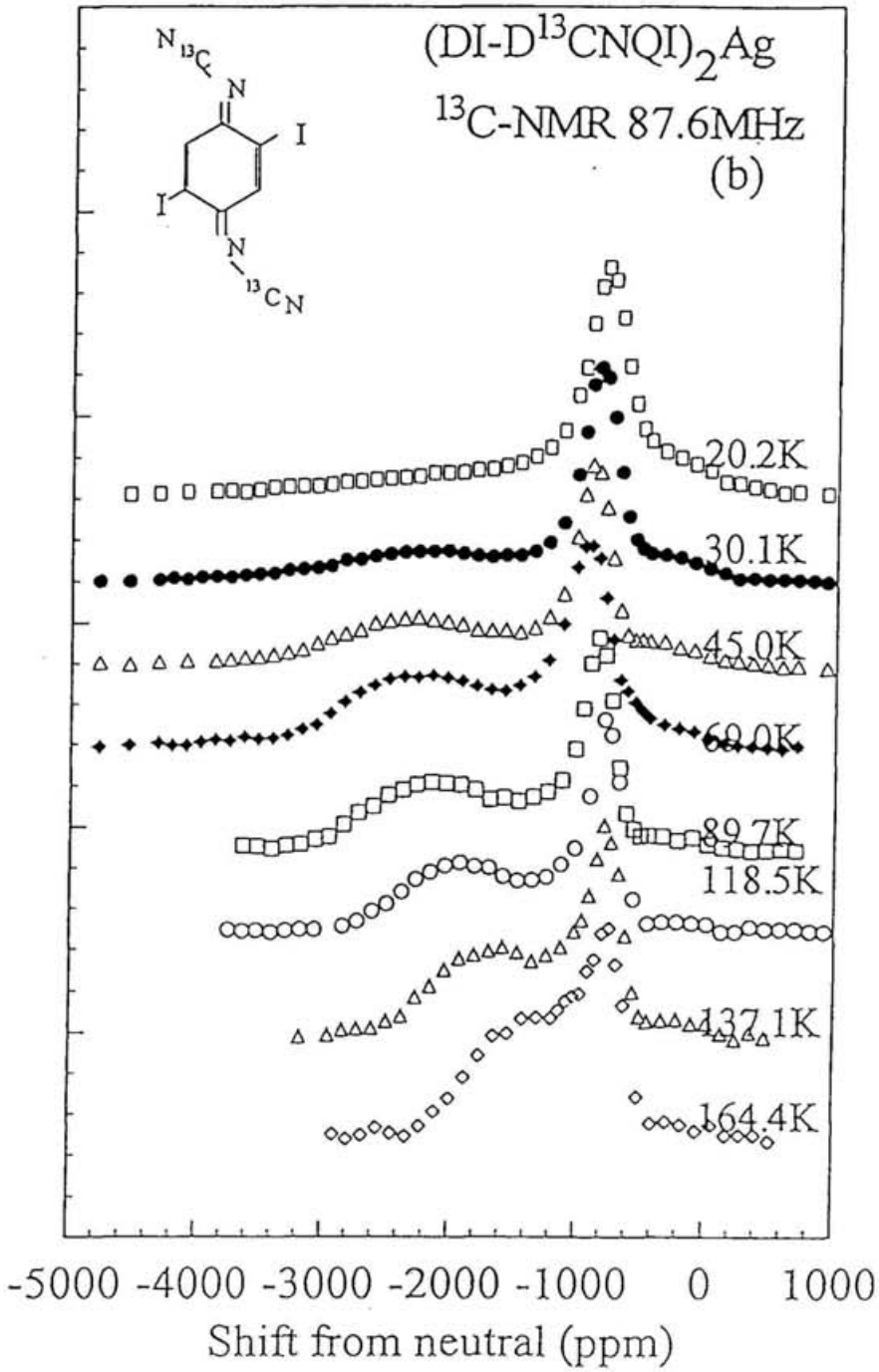
(DI-D13CNQI)2Ag
13C-NMR 87.6MHz
(b)
20.2K
30.1K
45.0K
60.0K
89.7K
118.5K
137.1K
164.4K
-5000 -4000 -3000 -2000 -1000 0 1000
Shift from neutral (ppm)

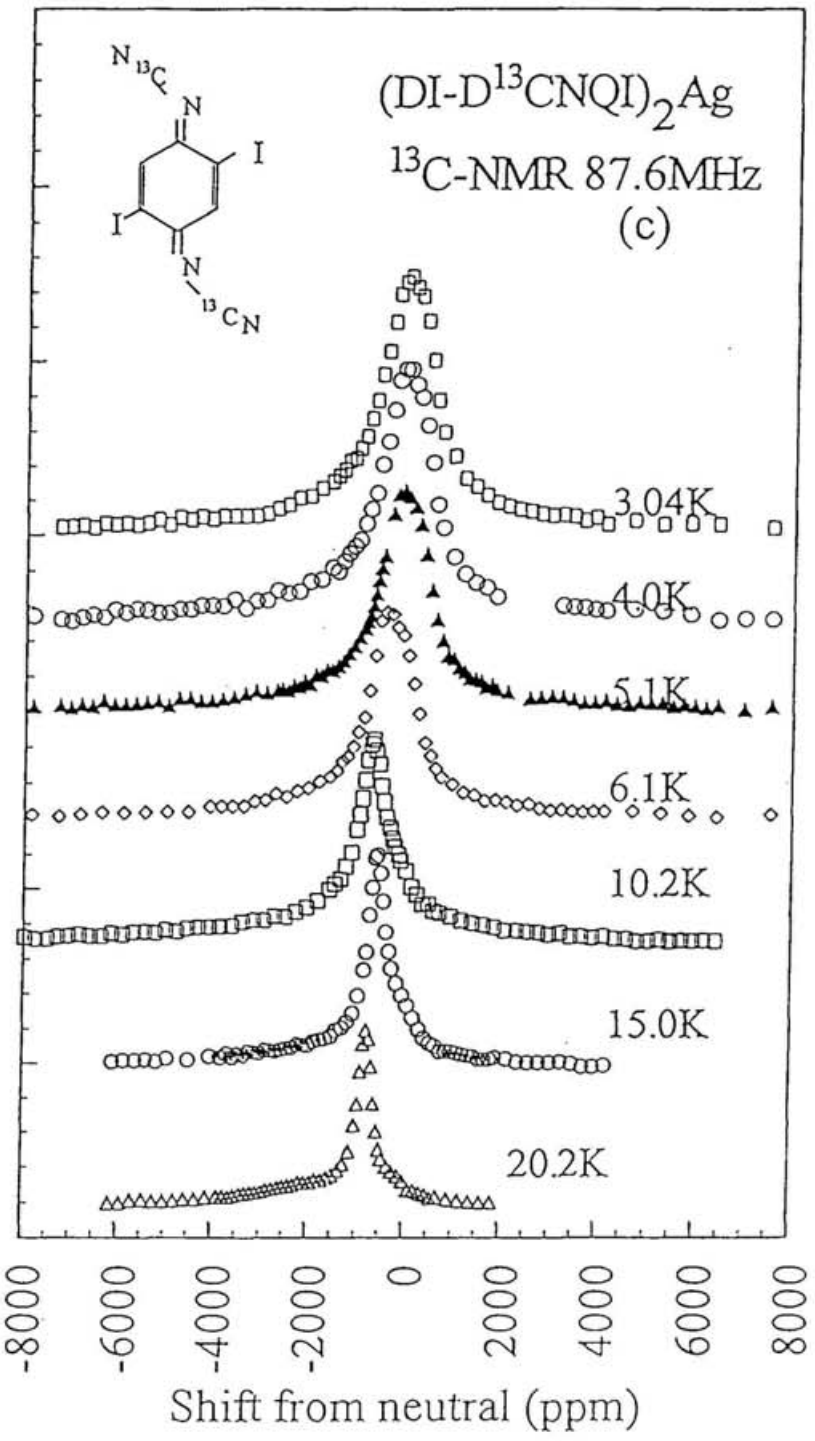
(DI-D13CNQI)2Ag
13C-NMR 87.6MHz
(c)
3.04K
4.0K
5.1K
6.1K
10.2K
15.0K
20.2K
-8000
-6000
-4000
-2000
0
2000
4000
6000
8000
Shift from neutral (ppm)

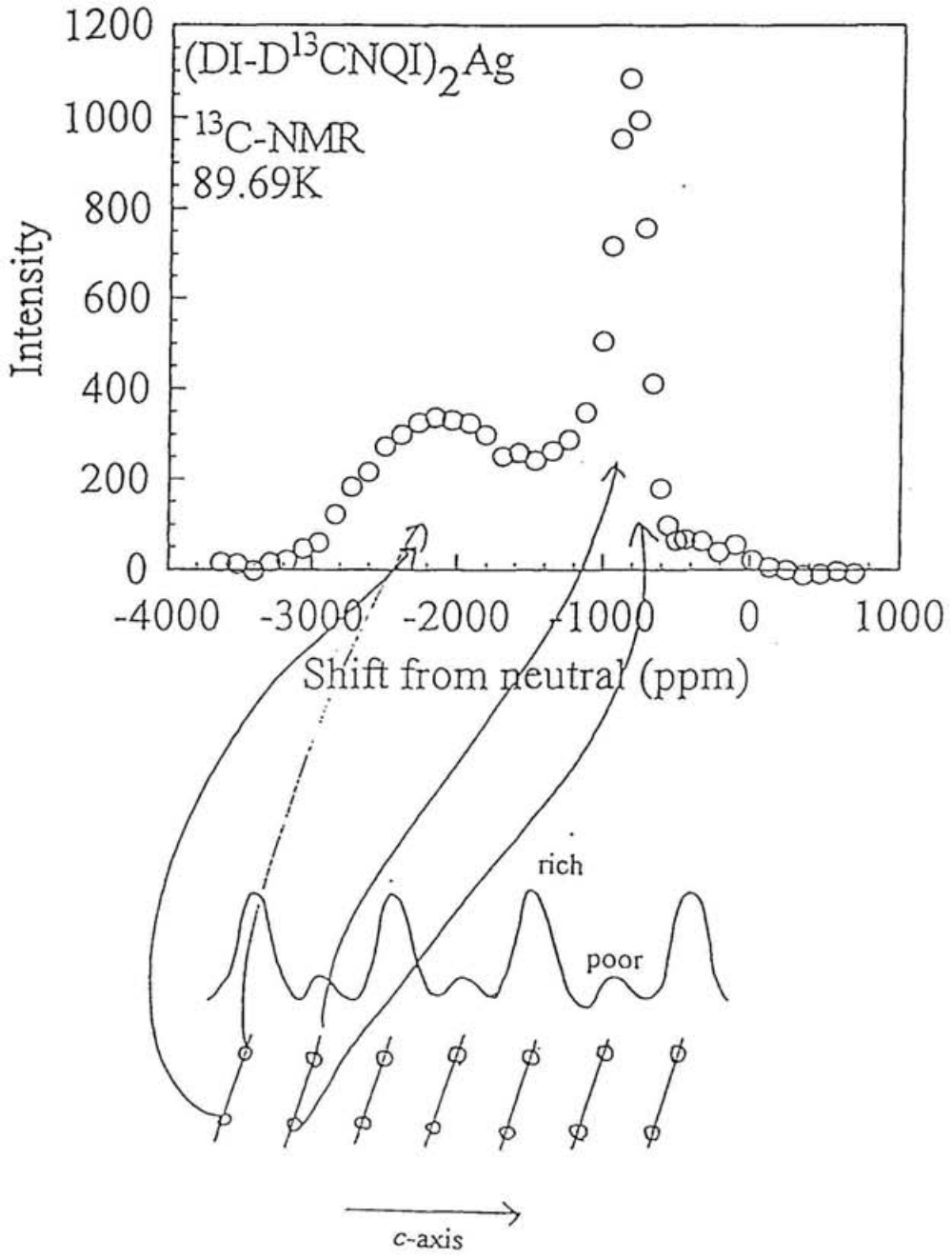

Fig. 3-4-2 Relation between ^{13}C-NMR spectrum and $4k_F$ charge ordering.

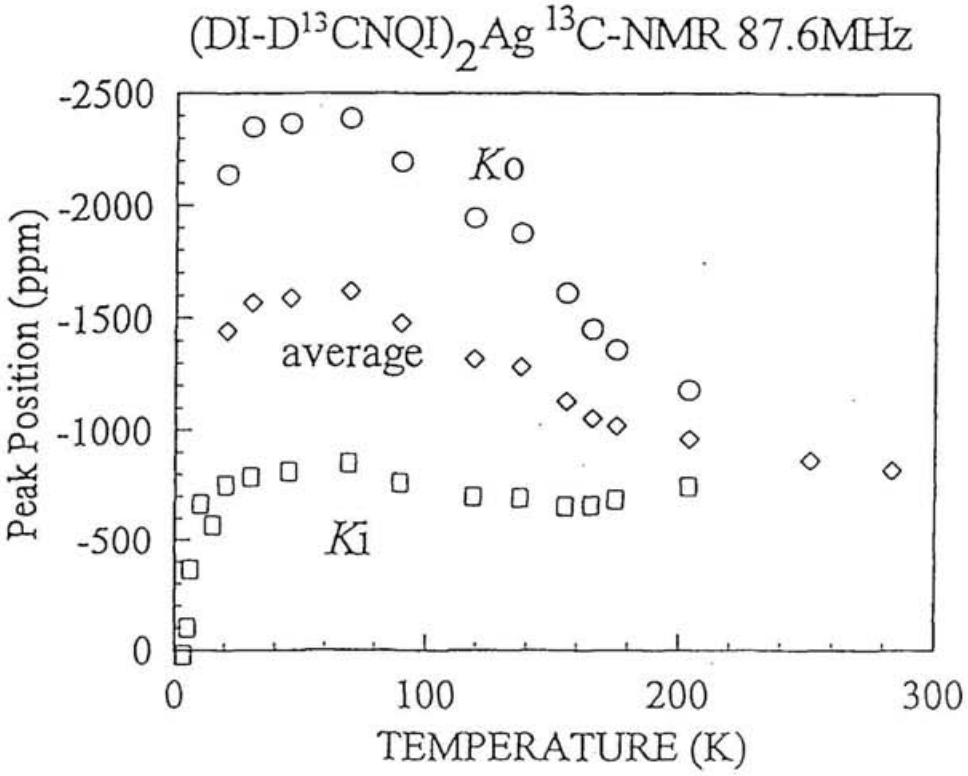

Fig. 3-4-3 Temperature dependence of the line position of ^{13}C-NMR spectra.

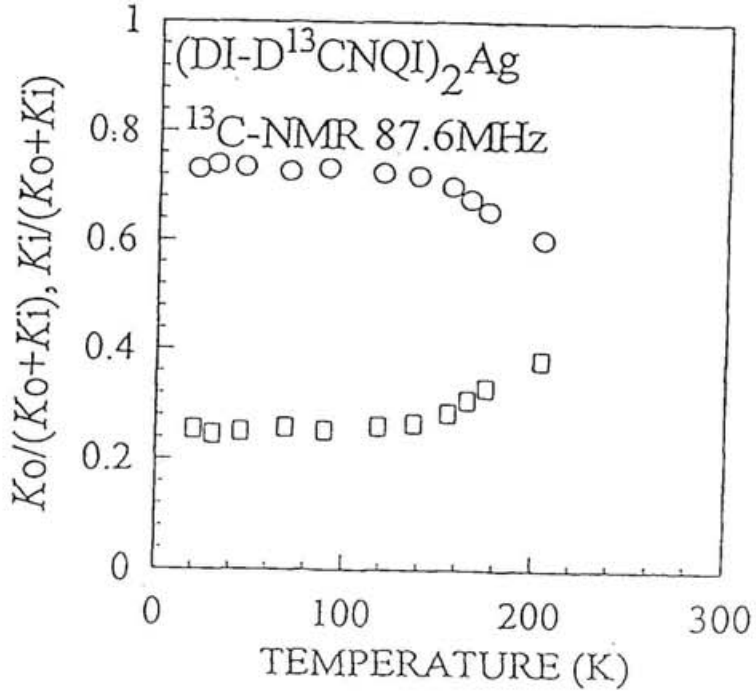

Fig. 3-4-4 Ki and Ko divided by (Ki+Ko) as a function of temperature.

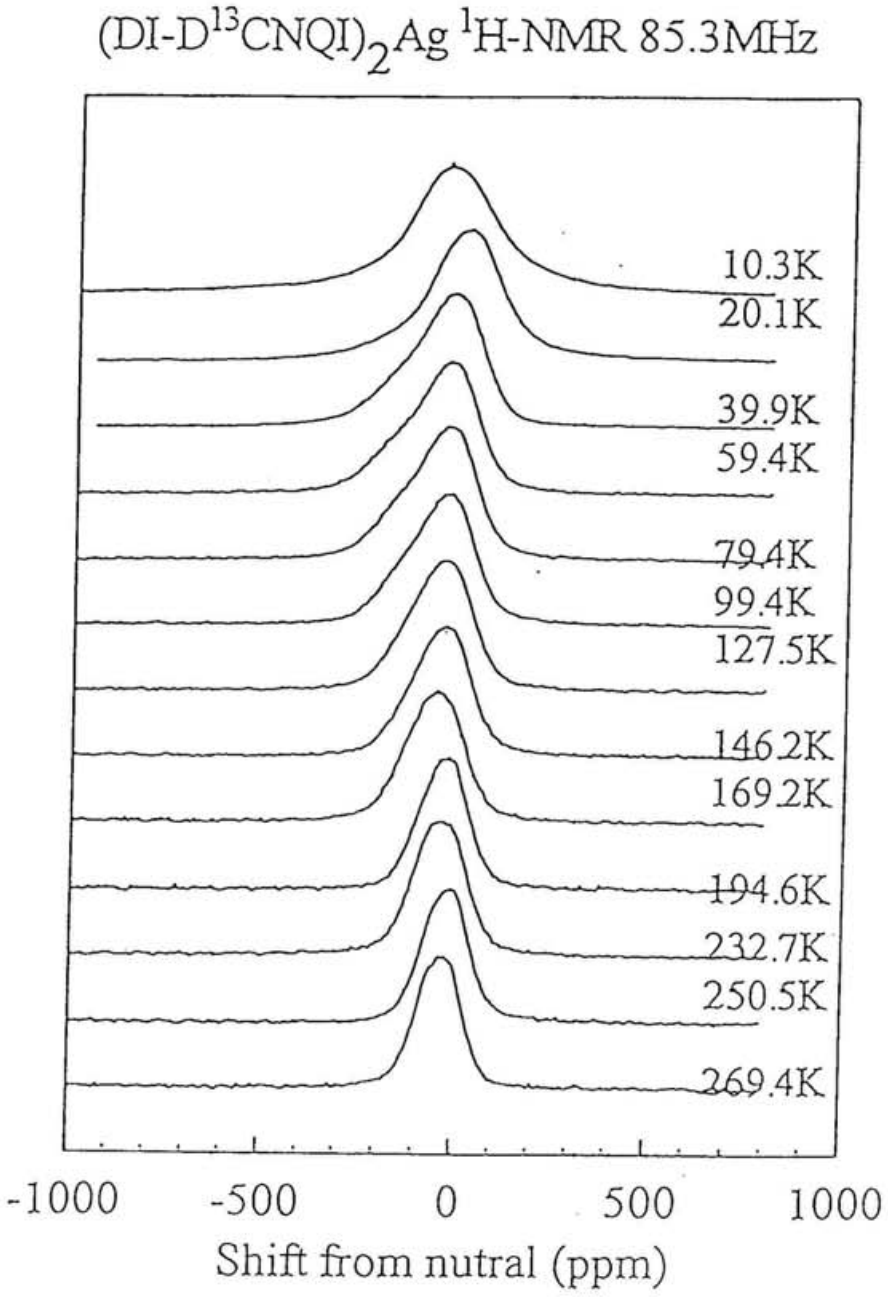

Fig. 3-5-1a) ^{1}H-NMR spectra of DI-Ag in paramagnetic state.

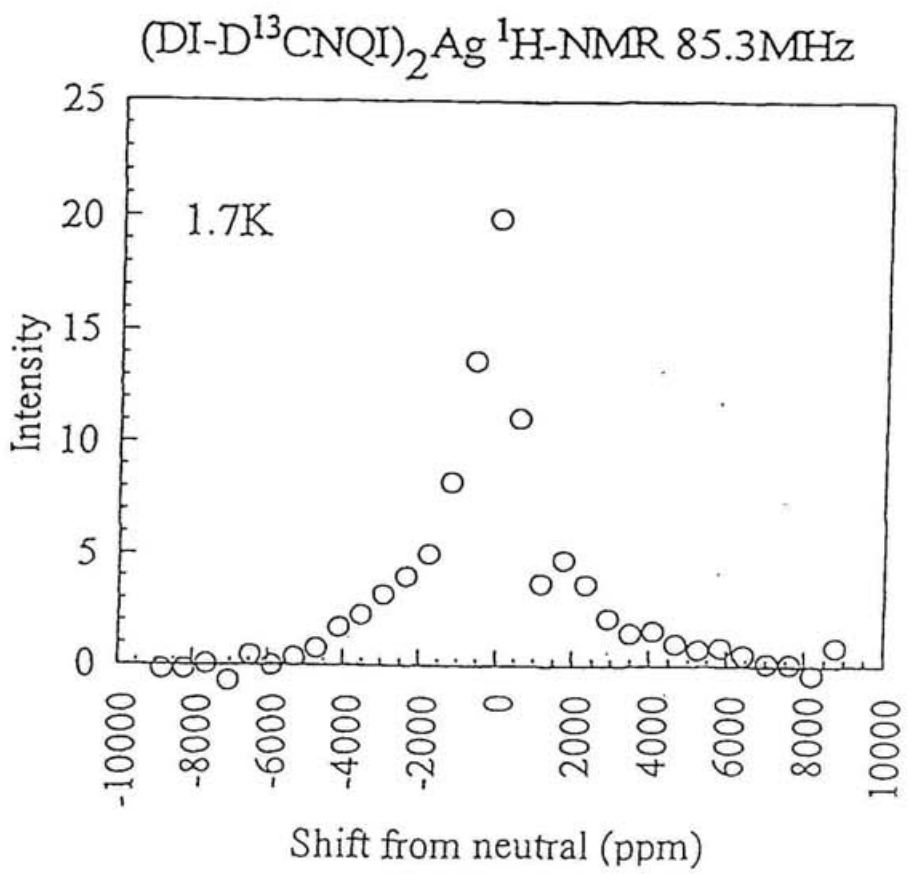

Fig. 3-5-1b) ^{1}H-NMR spectra of DI-Ag in AF state.

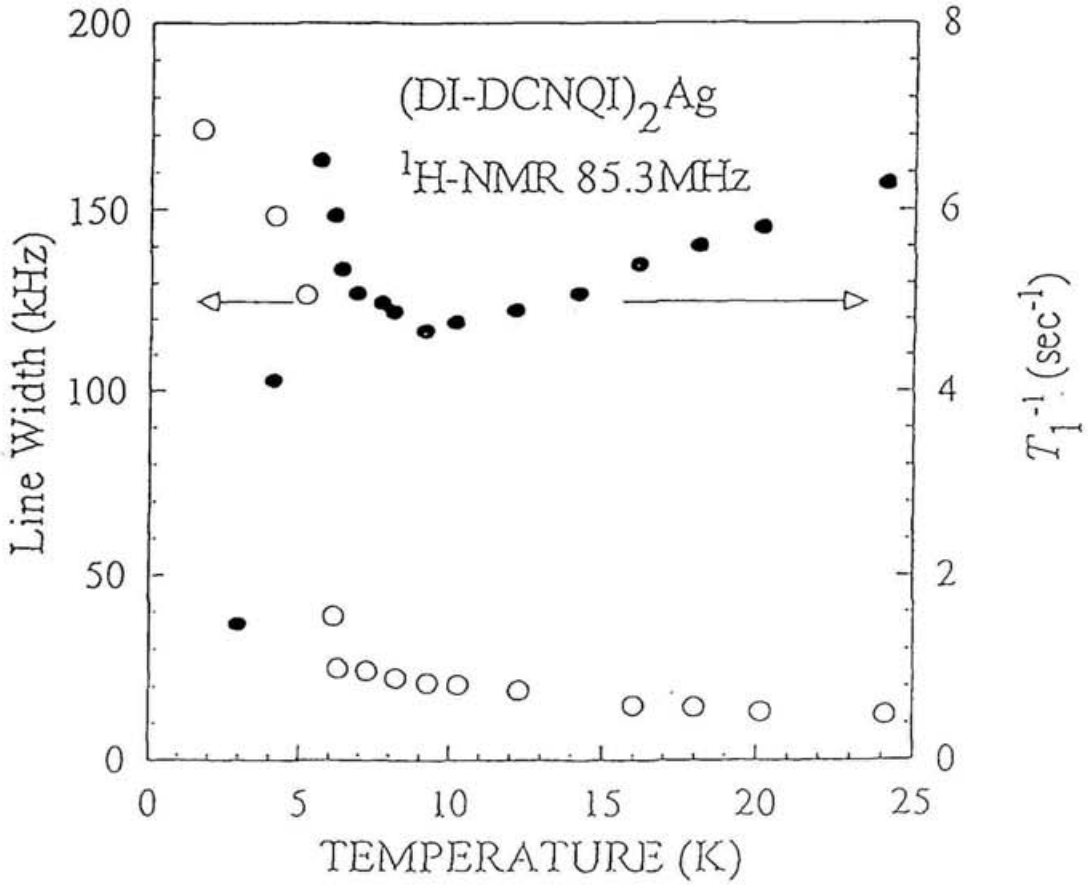

Fig. 3-5-2 Temperature dependence of the ^{1}H-NMR line width and T_1^{-1}.

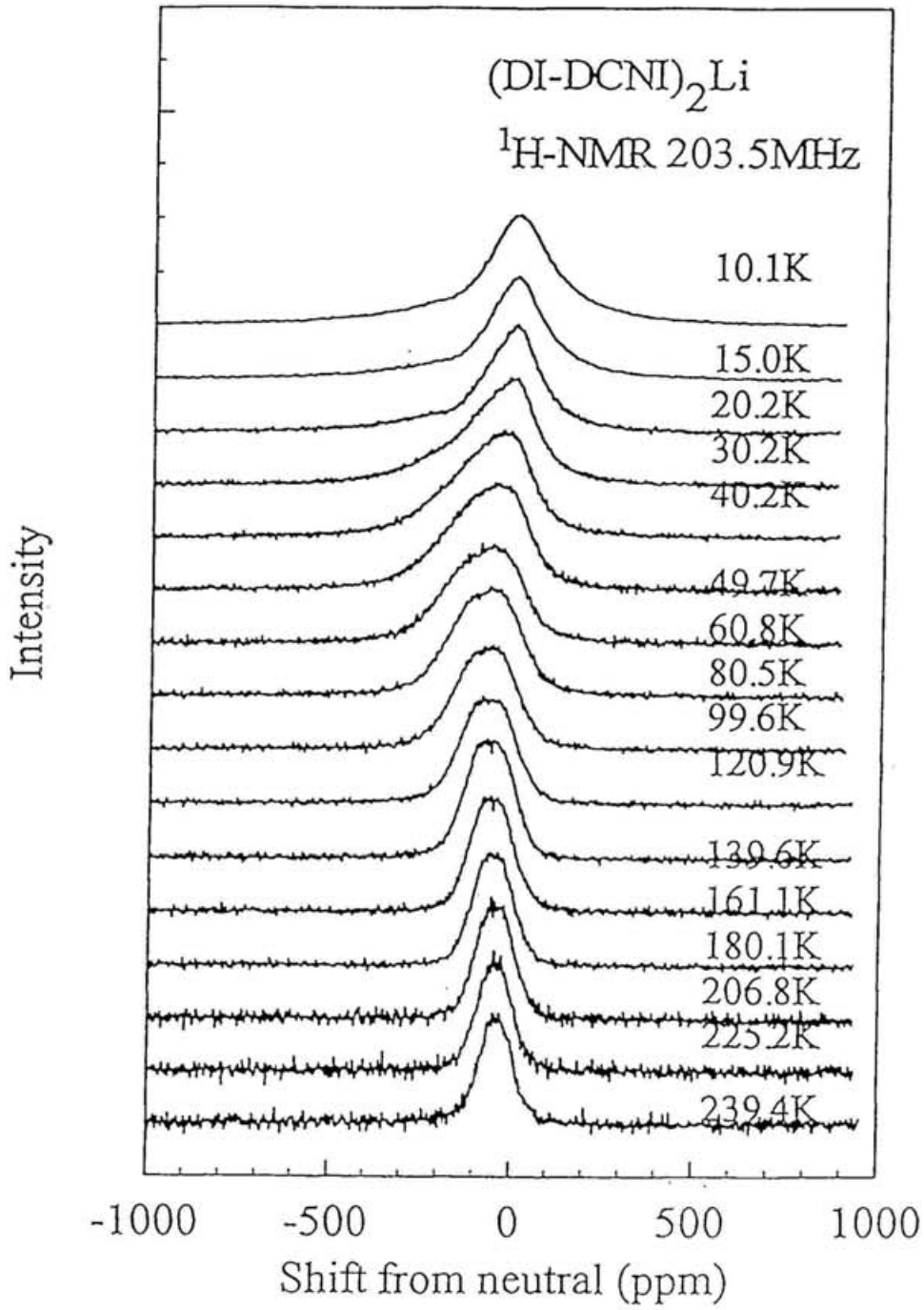

Fig. 3-6-1a) ^{1}H-NMR spectra of DI-Li.

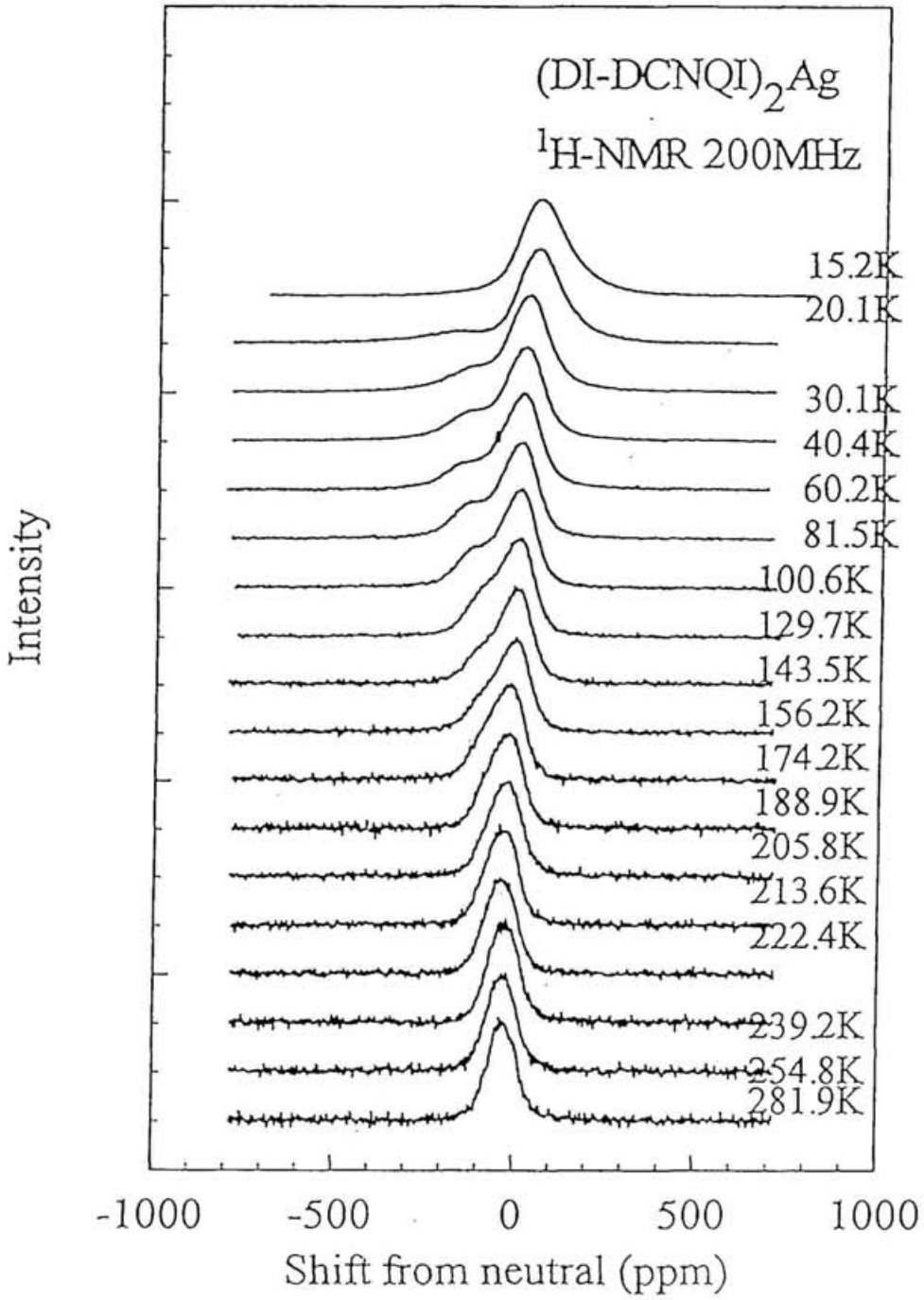

Fig. 3-6-1b) ^{1}H-NMR spectra of DI-Ag

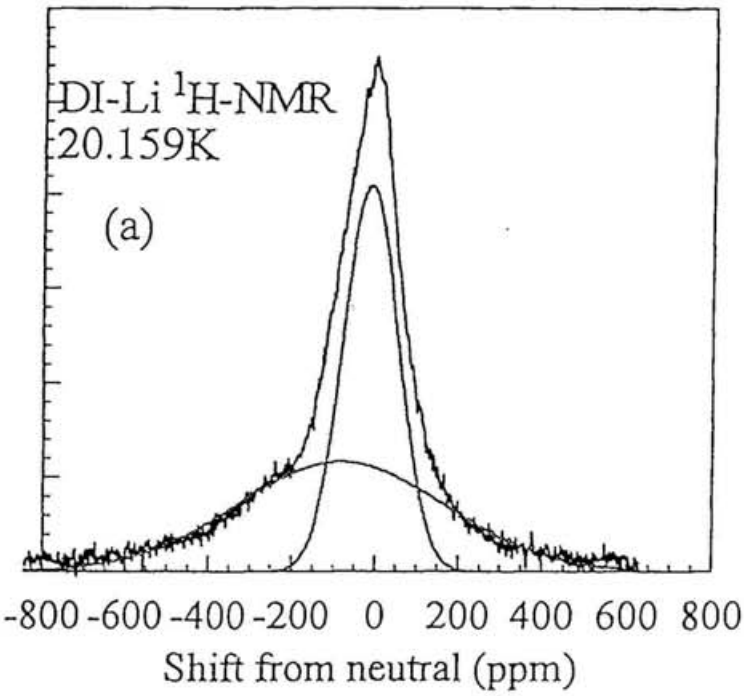

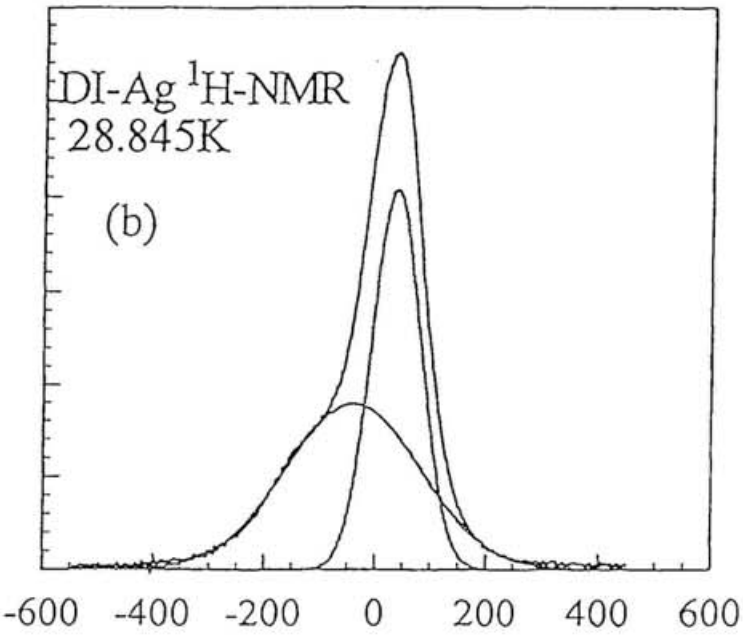

Fig. 3-6-2 ^{1}H-NMR spectra of DI-Li (a) and DI-Ag (b). The spectra are well reproduced by a sum of two Gaussian (solid lines).

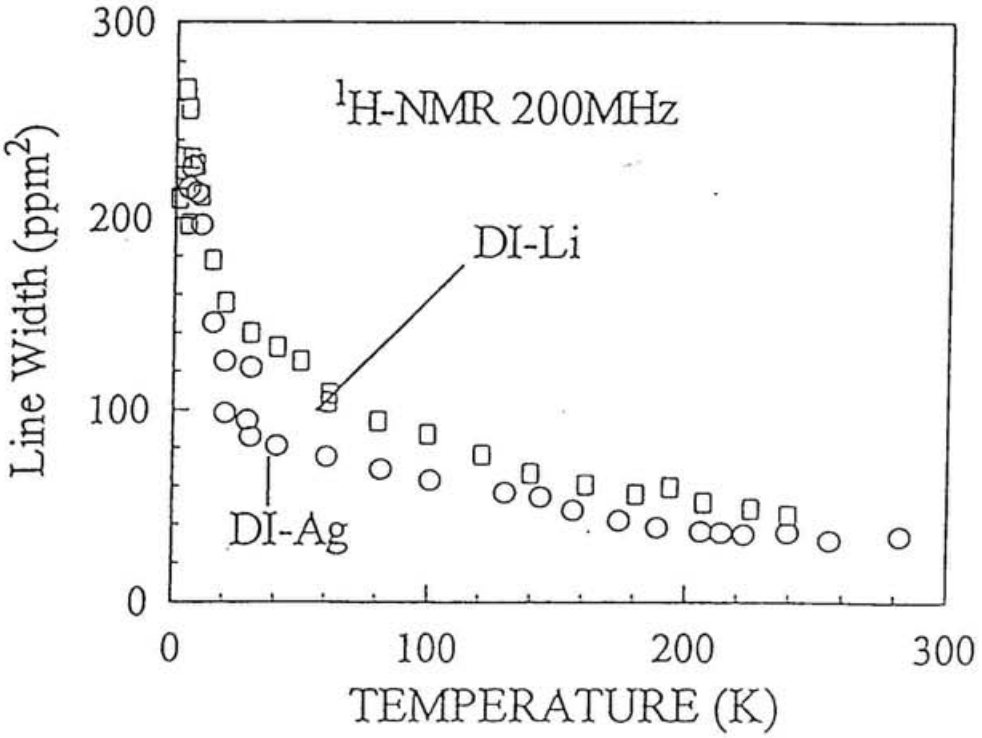

Fig. 3-6-3 Temperature dependence of ^{1}H-NMR linewidth of DI-Ag (circle) and DI-Li (square).

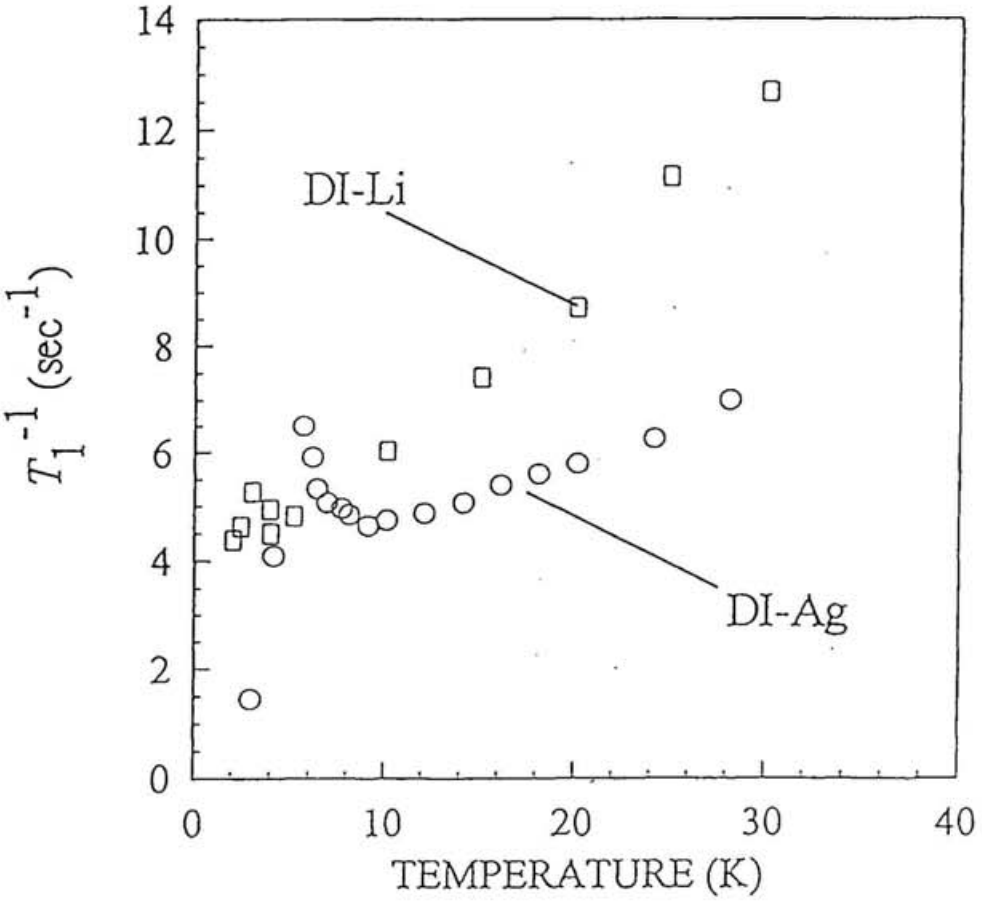

Fig. 3-6-4 Temperature dependence of T_1^{-1} of DI-Ag (circle) and DI-Li (square).

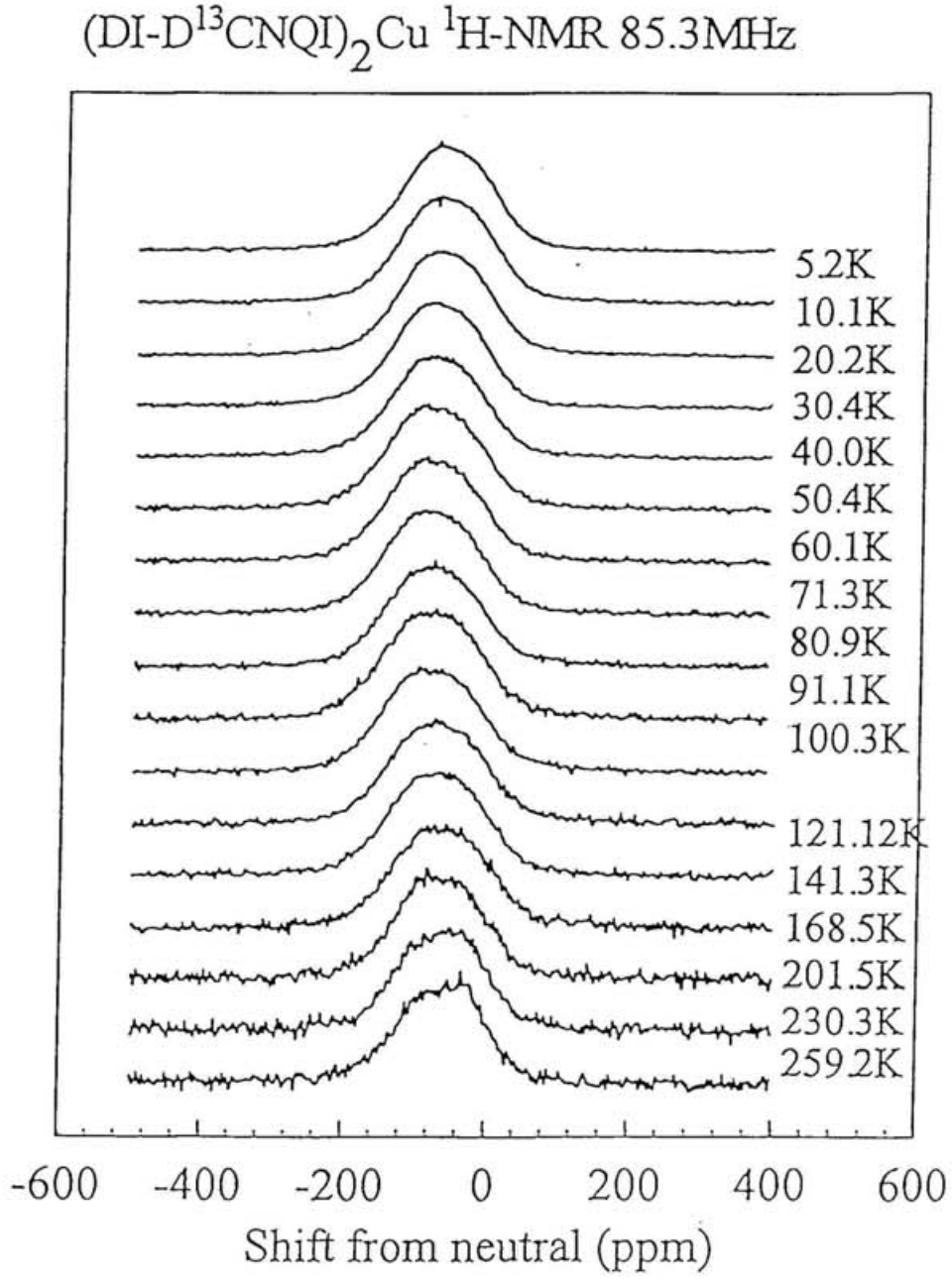

Fig. 3-7-1 ^{1}H-NMR spectra of DI-Cu

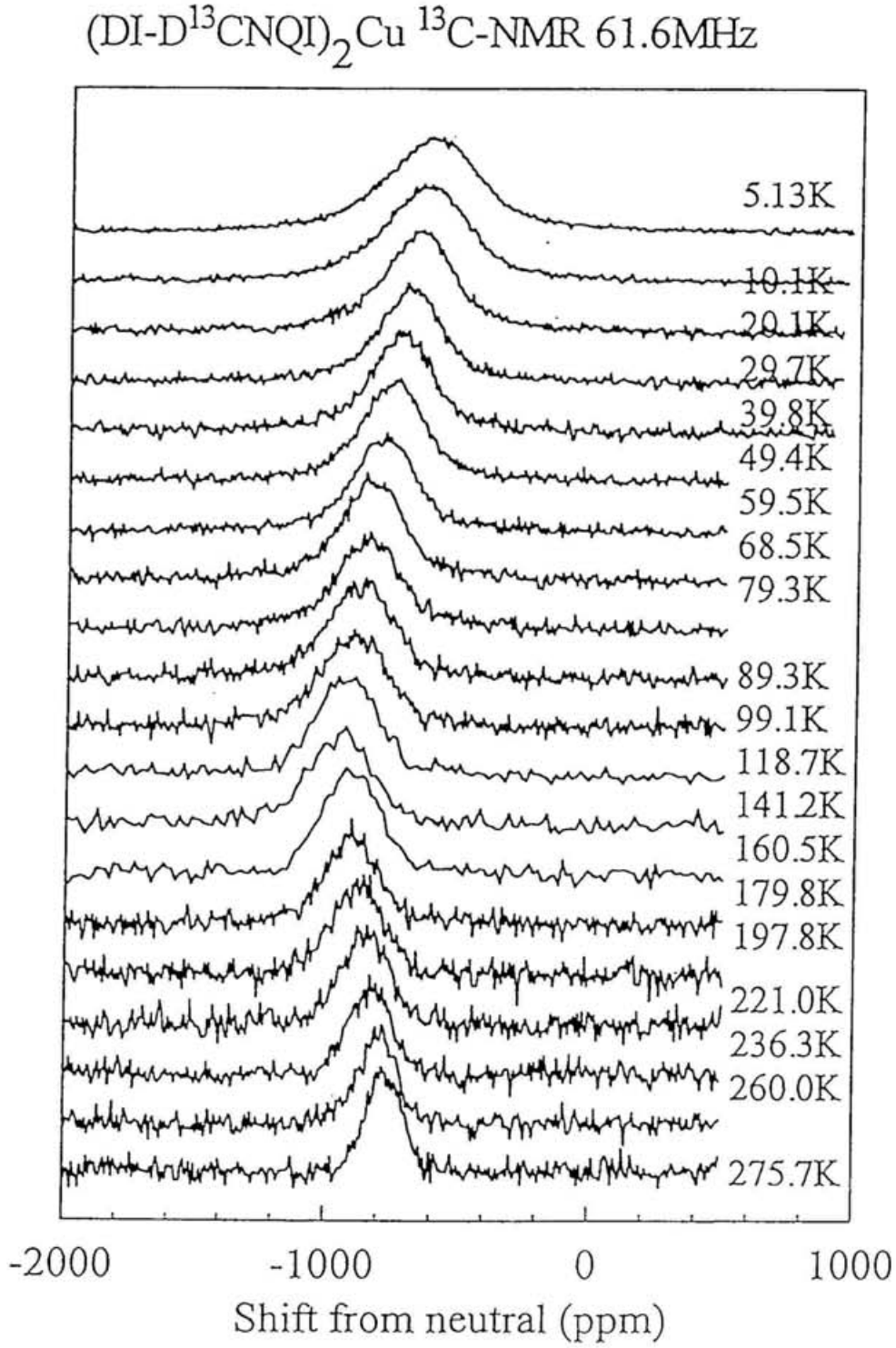

Fig. 3-7-2 ^{13}C-NMR spectra of DI-Cu.

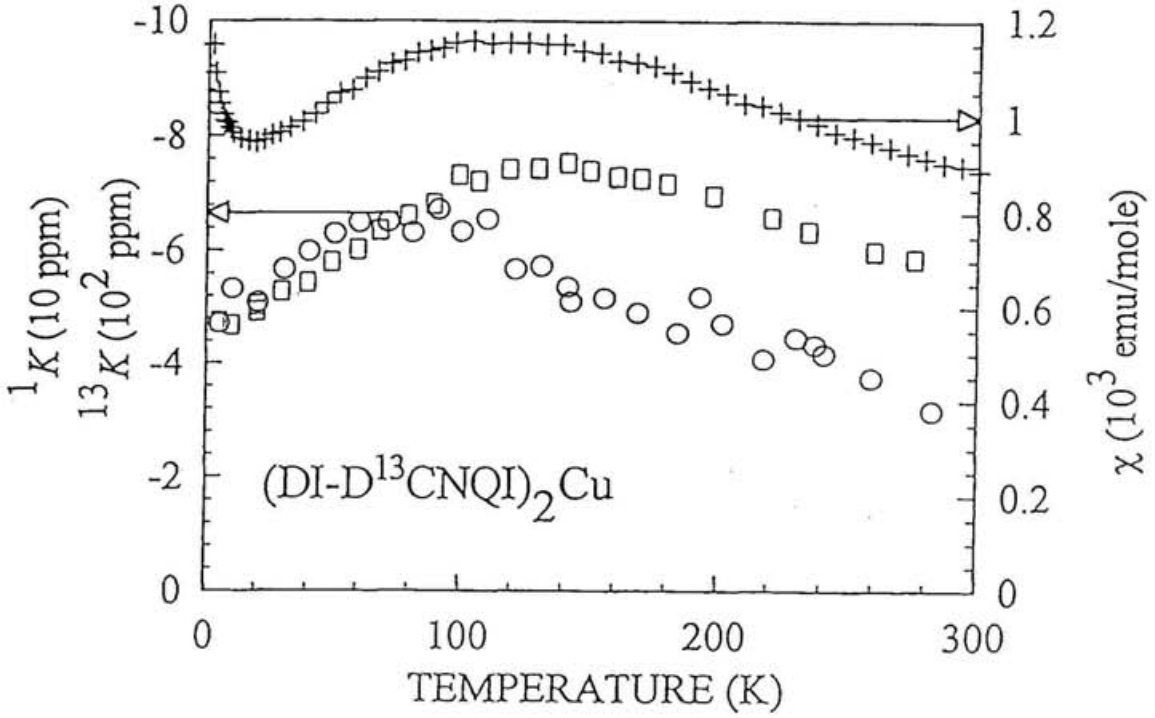

Fig. 3-7-3 Shift of ^{1}H-NMR and ^{13}C-NMR, ^1K and ^{13}K. The data of static χ are also plotted for comparison.

Chapter 4.

Carrier Doping to $(DMe\text{-}DCNQI)_2Li$; Electronic States of $(DMe\text{-}DCNQI)_2Li_{1-x}Cu_x$

4-1 Method

In general, doping is a useful method to control and provide novel electronic phases. This method should be promising for molecular conductors, as well as transition-metal oxides, which have been extensively studied. DMe-Li behaves as a 1D electronic system with a quarter filled π band. This system is metallic in a high temperature region, while it undergoes a non-magnetic (spin-) Peierls transition with freezing of $2k_F$ charge density wave (CDW) at 60K. On the other hand, DMe-Cu remains metallic down to low temperatures at ambient pressure in spite of the low-dimensional structure. The $3d$ orbital of Cu ions hybridize with LUMO of DMe-DCNQI and play a role of interconnecting the 1D π band. The valence of the Cu ions are around 4/3 (Cu^{1+}:$Cu^{2+}\cong$2:1) and the filling of 1D π band turns out to be about 1/3.

It is interesting to control the filling and/or dimensionality of the 1D π band by alloying of the metal ions, M, with different valency. Now, we consider alloy systems of Li and Cu as M. So, Cu doping to the M site in the DMe-Li is expected to cause some change of filling of 1D π band and generate 3D character through the hybridization of the Cu 3d orbital with the π orbital. In this chapter, observation of the effect of doping to the 1D electronic system is described.

The Alloy systems, $(DMe\text{-}DCNQI)_2Li_{1-x}Cu_x$, with a systematic series of composition were synthesized and characterized by the ρ, χ and ^{13}C-NMR measurements. In chapter 4-2, preparation and evaluation of homogeneity of the samples are described. Conducting and magnetic properties are described in chapter 4-3, and further informations of the electronic states obtained by ^{13}C-NMR are presented in chapter 4-4.

4-2 Sample preparation

The crystals of $(DME\text{-}DCNQI)_2Li_{1-x}Cu_x$ were prepared by chemical reduction using (n-Bt_4N)I (n-tetrabuthylammonium iodide) from acetonitril (CH_3CN) solution of DME-DCNQI and mixture of $LiClO_4$ and $(Et_4N)_2CuBr_4$ (where Et_4N is tetraethylammonium)[1]. The content x in $(DME\text{-}DCNQI)_2Li_{1-x}Cu_x$ was determined by ICP-AAS[2]. A relation between the values of x in preparation and those observed by ICP is shown in Fig. 4-2-1. In a region of small x, the Cu is incorporated more than its content in preparation. For large x, the resultant x is nearly equal to that in preparation. Samples with $x = 0$ (Li salt), 0.18, 0.33, 0.49, 0.70 and 1.0 (Cu salt) were prepared. It is important to examine the homogeneity of the samples in case of study of the alloy system. The ^{13}C-NMR spectrum of the systems at room temperature are shown in Fig. 4-2-2. The difference of the line positions between the systems of $x = 0$ and 1.0 reflects difference of the ^{13}C hyperfine coupling constant and local spin susceptibility. The spectra of the alloy systems are somewhat broad but forms a single peak. If the alloy systems had phase separation, e.g. a mixture of the salts of $x = 0$ and 1.0, the spectra would form a double peak structure. A microscopic difference of the metal ions in neighbor of the ^{13}C sites, namely Li or Cu, which is inherent in the alloy systems, gives a variation of the hyperfine coupling constant of ^{13}C and may contribute to the broadening of the spectra. Note that the variation of the hyperfine coupling does not mean inhomogeneity of the electronic state. In addition, the recovery curves of nuclear magnetization in the alloy systems were nearly single exponential functions as shown in Fig. 4-2-3 while the T_1^{-1} of the two limiting salts of $x = 0$ and 1.0 are quite different. These observations suggest that there is

no serious inhomogeneity in the samples. More or less fluctuations in x over the sample volume cannot be ruled out.

4-3 Conducting and Magnetic Properties

In this chapter, the conducting and magnetic properties of (DMe-DCNQI)$_2$Li$_{1-x}$Cu$_x$ are described. Figure 4-3-1 shows the temperature dependence of resistivity, ρ. All the systems behave metallic in high temperatures (T > 100 K). The systems with x up to ~0.3 are insulating at low temperatures. On the other hand, the systems with x > 0.5 are metallic in the whole temperature range without any anomaly. The resistive transition temperature seems to decrease with increasing x up to ~0.3 but is not well-defined as the case of x = 0. The system around x = 0.3 is the boundary between metal-insulator transition.

In what follows, the mechanism of the metal-insulator transition or crossover is discussed. The two limiting cases of x=0 and 1 are an one-dimensional (spin-)Peierls insulator and a three-dimensional metal with π-d hybridization, respectively. Doping of Cu causes the following three effects on the electronic system; the first is lifting of dimensionality by interchain coupling due to the π-d hybridization, the second is a change of filling of the π band between a quarter and a third, and the third is introduction of randomness. With x varied, these three processes are going on, as depicted in Fig. 4-3-2. If DMe-Li is viewed as a 1-D Peierls insulator driven by the Fermi surface nesting, the first effect acts against nesting and tends to lead the system into the 3-D metals with x increased. Alternatively if DMe-Li is viewed as a 1-D spin-Peierls insulator, the second

effect makes the system metallic with x increased. In any event, the former two effects act in favor of the metallic state. On the other hand, the third effect (disorder) should be enhanced in the middle range of x. After all, the change of the electronic state results from the interplay between these effects. The systems with $x = 0.33$, 0.49 and 0.70 have a finite metallic resistivity in the low-temperature limit but shows lower residual resistivity ratios than that of the system with $x = 1.0$. (Near $x = 0.5$, for example, it is an interesting expectation that a novel ordered state of Li and Cu may appear. However, the resistivity behavior of the system with $x = 0.49$ shows no sign of this state.) They can be disordered 3-D metals. However, the system with $x = 0.18$ is a nonmetal but has no such an anomaly as the system with $x = 0$. This feature suggests an disorder-induced insulator, which is consistent with residual spin susceptibility (described below) even at low temperatures for this system. Since the dimensionality of the electronic state is crucial for the effect of disorder, the present metal-insulator transition is reasonably addressed as an issue of the dimensional crossover of the electronic state in presence of disorder.

Figure 4-3-3a) shows the temperature dependence of χ. The diamagnetic core contributions were calculated according to Pascal's law; -9.15×10^{-5}, -0.6×10^{-5} and -1.2×10^{-5} emu/mole for DMe-DCNQI, Li^+ and Cu^+, respectively. The Curie contributions was observed in all systems. The Curie constant, C, and the spin fraction, A, of each system are listed in table 4-1. It is obvious that A is much smaller than x and there is no correlation between them. This fact indicate that the Curie term does not come from the doped Cu but from some impurities. Therefore, the doped Cu ions turn out to carry no localized spins even in the insulating phase and suggested to be monovalent or mixed-valent. Since the Curie terms are so small as shown in Fig. 4-3-2, it is reasonable to

consider that there is no serious influence on the electronic states. The susceptibility after subtraction of the Curie term is shown in Fig. 4-3-3b).

Table 4-1. Low-temperature Curie term. A is the spin fraction per formula unit.

x	C(emu/mole K)	A
0 (Li salt)	7.28E-4	0.0019
0.18	1.66E-3	0.0044
0.33	1.44E-3	0.0038
0.49	5.46E-4	0.0015
0.70	8.03E-4	0.0021
1.0 (Cu salt)	1.45E-3	0.0039

The abrupt decrease of χ at 60 K in the system of $x = 0$ (Li salt) is due to the freezing of $2k_F$ CDW. A systematic change of χ with Cu doping in a low temperature region ($T < 100$ K) is seen. Up to $x \sim 0.3$, where the system is nonmetallic in resistivity, the susceptibility anomaly occurs around 45 - 60 K with a finite low-temperature value of χ, which is correlated with x as seen in Fig. 4-3-4. This behaviors are not compatible with the (spin-) Peierls non-magnetic state, but reconciled with disorder-induced electron localization with finite density of states at Fermi level. The anomaly around 45-60 K may be interpreted as the imperfect nesting. Above $x \sim 0.3$, there is no anomaly in susceptibility, which shows Pauli-like. This perfect suppresion of the nesting, which shows 3D nature of the electronic state, coincides with the appearance of the metallic resistivity. This is a

manifestation of the ineffectiveness of randomness to electron localization in higher-dimensional system.

4-4 ^{13}C-NMR study

In this chapter, the ^{13}C-NMR results of the doped systems are presented. The transport measurements revealed that the systems are insulating at low temperatures up to $x \sim 0.3$ while the systems with $x > 0.5$ are metallic in the whole temperature range.

The ^{13}C-NMR spectra of the systems with $x = 0$ (Li slat), 0.18, 0.33, 0.49, 0.70 and 1.0 (Cu salt), are shown in Fig. 4-4-1a), b), c), d), e) and f), respectively. The structure of the ^{13}C-NMR spectra of the $x = 0$ system is markedly changed with temperature varied. The spectra in the metallic state at high temperatures are symmetric. Well below the (spin-) Peierls transition temperature, T_P, of 60 K, there is no contribution of electron spins to the shift and therefore the asymmetry is due to the anisotropy in the chemical shift of DMe-DCNQI molecules. The samples of $x = 0.18$ and 0.33 also show the similar temperature profiles of spectra. However, the characteristic temperature, where the symmetric spectrum changes to the asymmetric one, slightly shifts to a lower temperature of 40 -50 K and the lineshape of the spectra at the lowest temperature is different from the perfectly nonmagnetic case of $x = 0$. These behaviors are consistent with the inperfect nesting postulated in the previous section. On the other hand, the spectra of the systems with $x > 0.5$ remain symmetric down to low temperatures, providing microscopic evidence of absence of nesting.

The ^{13}C-NMR relaxation rate, T_1^{-1}, is shown in Fig. 4-4-2. For $x = 0$, $(T_1T)^{-1}$ decreases

abruptly below T_P of 60 K and vanishes at low temperatures due to opening of a spin gap. For x = 0.18 and 0.33, T_P seems to decrease down to 40 -50 K, below which $(T_1T)^{-1}$ approaches a finite value. This value increases with x. The overall feature of the results for $x \leqq 0.3$ is consistent with a picture of imperfect nesting and electron localization discussed above. In the metallic state, the $(T_1T)^{-1}$ has positive temperature dependence and the magnitude is clearly correlated with the doping content. Especially, for the systems of $x > 0.5$, $(T_1T)^{-1}$ does not exhibit any anomaly in the whole temperature range and converges into a value of about 0.03 $sec^{-1}K^{-1}$ in the low temperature limit, irrespectively of x. This systematic deviation from $(T_1T)^{-1}$ = const. is an indication that the doping causes some change in the electronic states, particularly in the excitation spectrum even in the metallic region.

4-5 Summary

The electronic states of (DMe-DCNQI)$_2$Li$_{1-x}$Cu$_x$ has been studied by resistivity, susceptibility and ^{13}C-NMR measurements. The system with x = 0 (Li salt) shows abrupt decrease of conductivity, susceptibility, shift and $(T_1T)^{-1}$ due to the freezing of $2k_F$ CDW. The results of the systems up to $x \sim 0.3$ are characterized by the nonmetallic conductivity and incomplete decrease of the susceptibility, shift and $(T_1T)^{-1}$ at a decreased temperature of 40 -50 K. These behaviors can be understood by the imperfect Fermi surface nesting due to the π-d hybridization and disorder-induced electron localization. When x exceeds 0.5, the systems remain metallic down to low temperatures without any sign of the nesting. This indicates considerable degree of three-dimensionality of the electronic state,

where the randomness loses the role of electron localization. In high temperature region ($T > 100$ K) of all systems are metallic. The large deviation of $(T_1T)^{-1}$ from the relation, $(T_1T)^{-1}$ = constant, expected in noncorrelated metal strongly indicate a change of the metallic nature, with x varied.

References

1. R. Kato *et al.*, Solid State Commun. **85**, 831 (1993); R. Kato private communication
2. Inductively Coupled Plasma Atomic Emission Spectrometer
3. T. Takahashi *et al.*, unpublished
4. G. Soda *et al.*, J. Phys. (paris) **38**, 931 (1977)

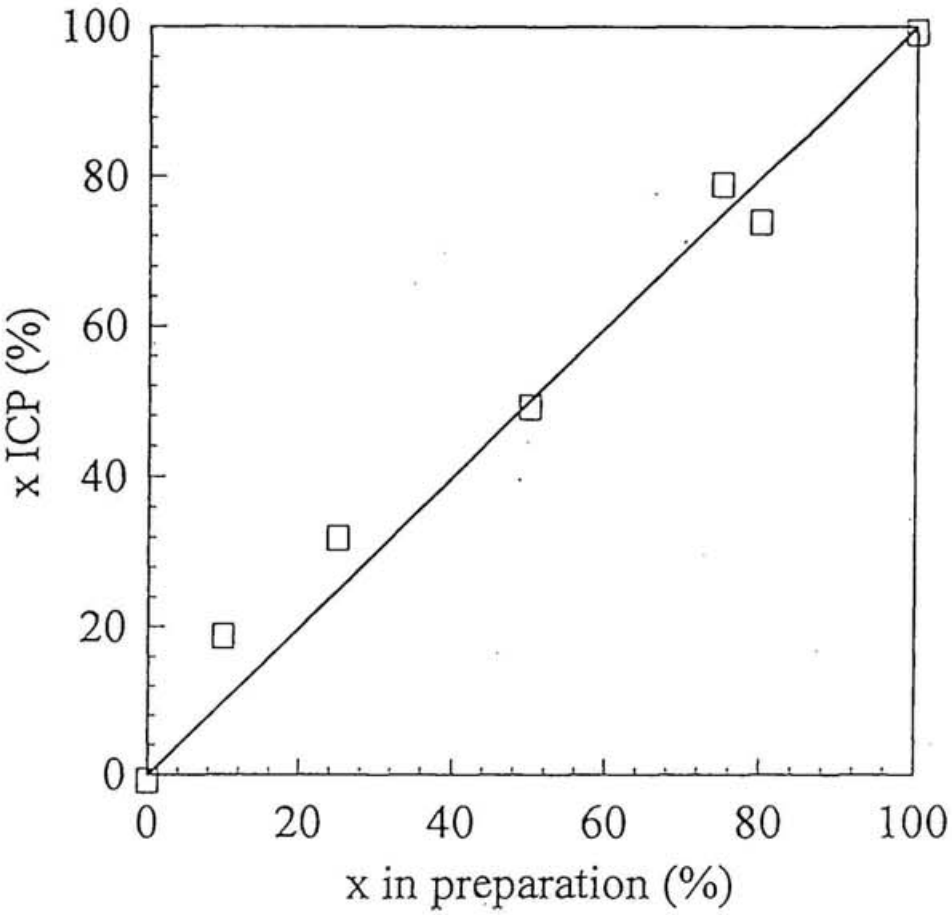

Fig. 4-2-1 A relation between the values of x in preparation and those observed by ICP.

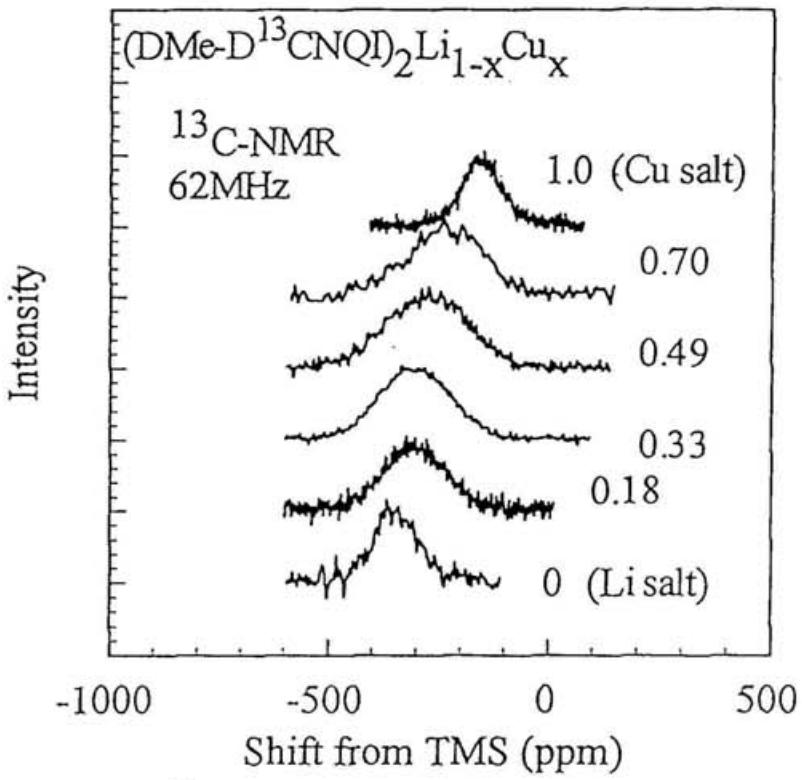

Fig. 4-2-2 ^{13}C-NMR spectra at room temperature of each system.

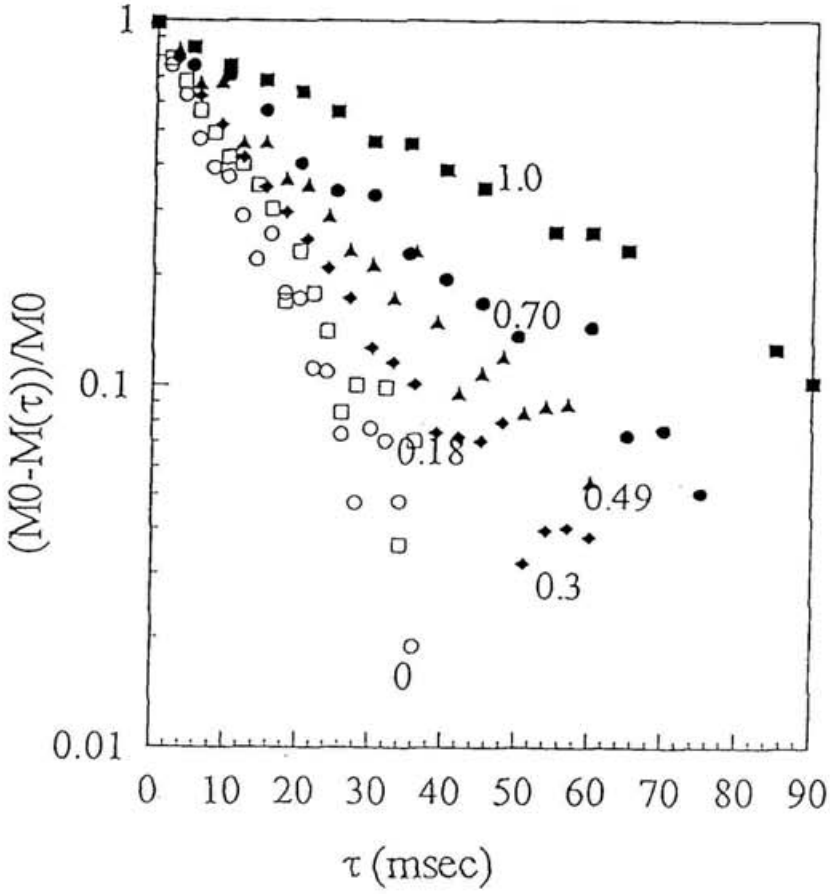

Fig. 4-2-3 ^{13}C-NMR recovery curve at room temperature of each system.

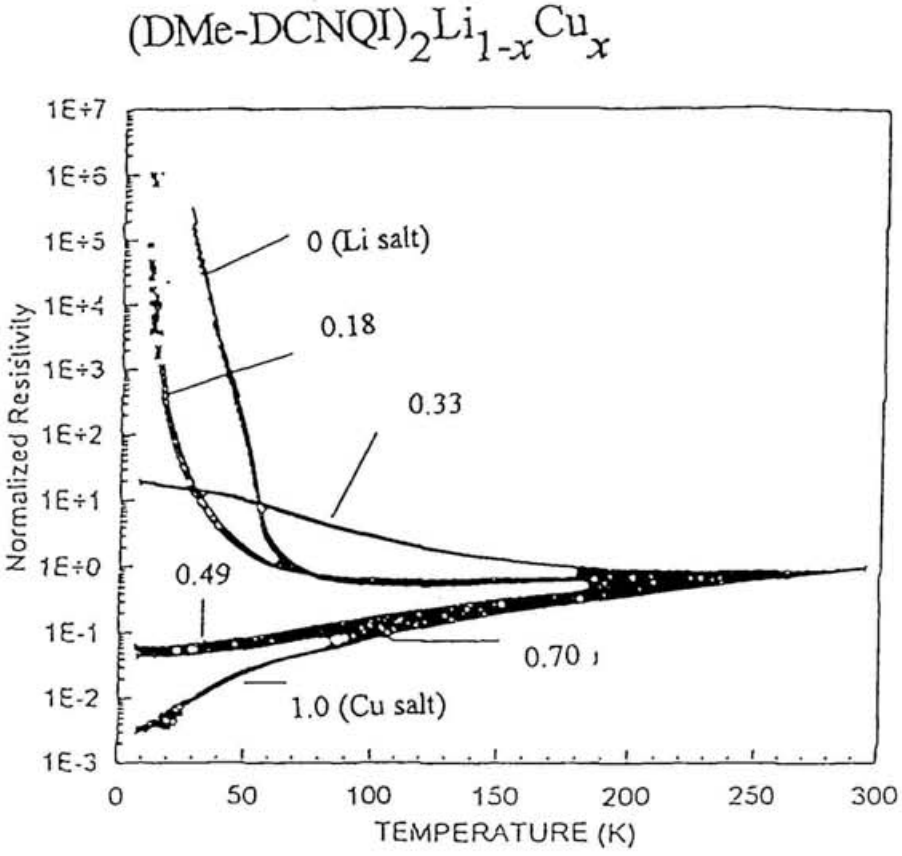

Fig. 4-3-1 Temperature dependence of ρ of each system.

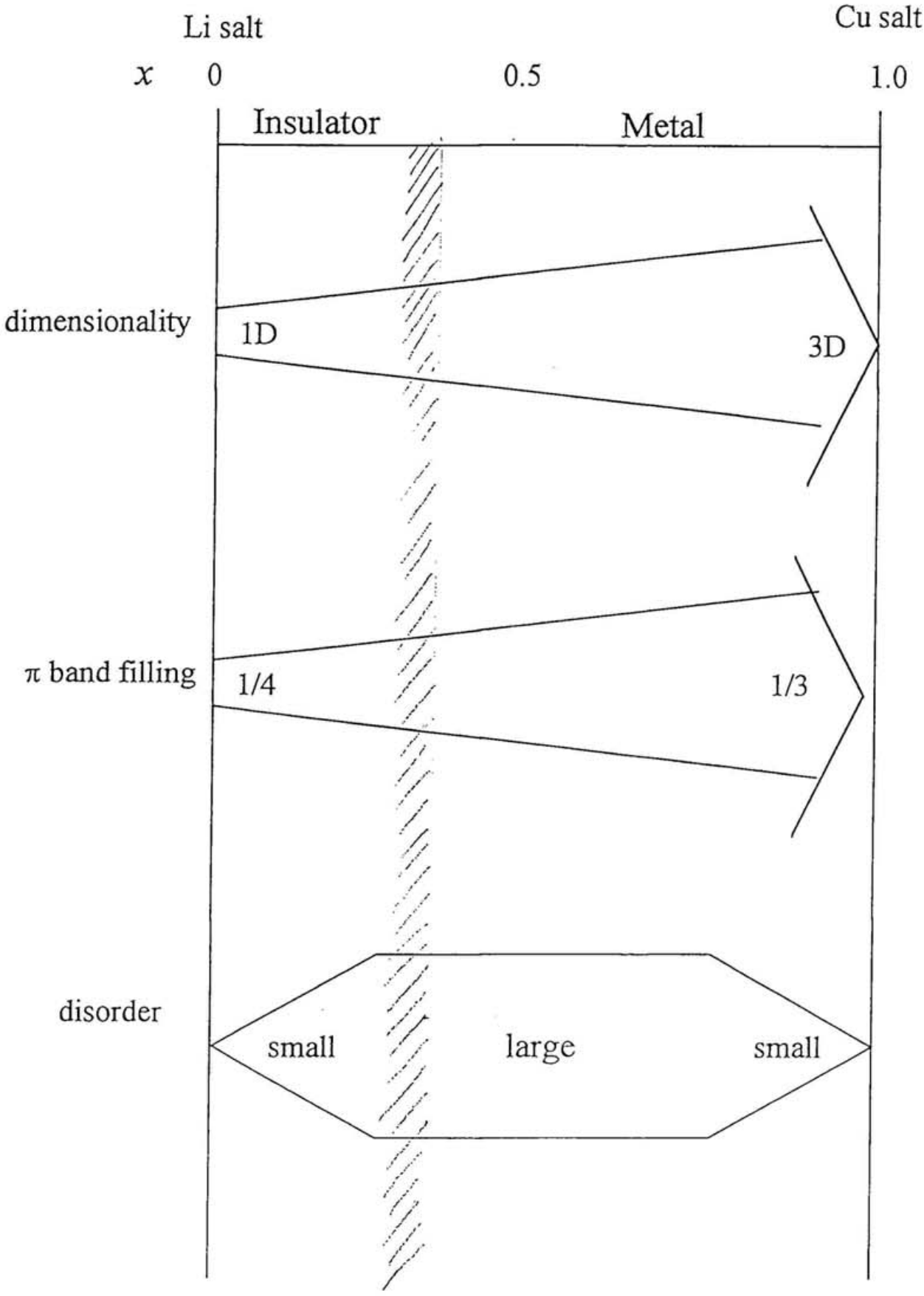

Fig. 4-3-2 Schematic relationship between x and the dimensionality, π band filling and degree of disorder.

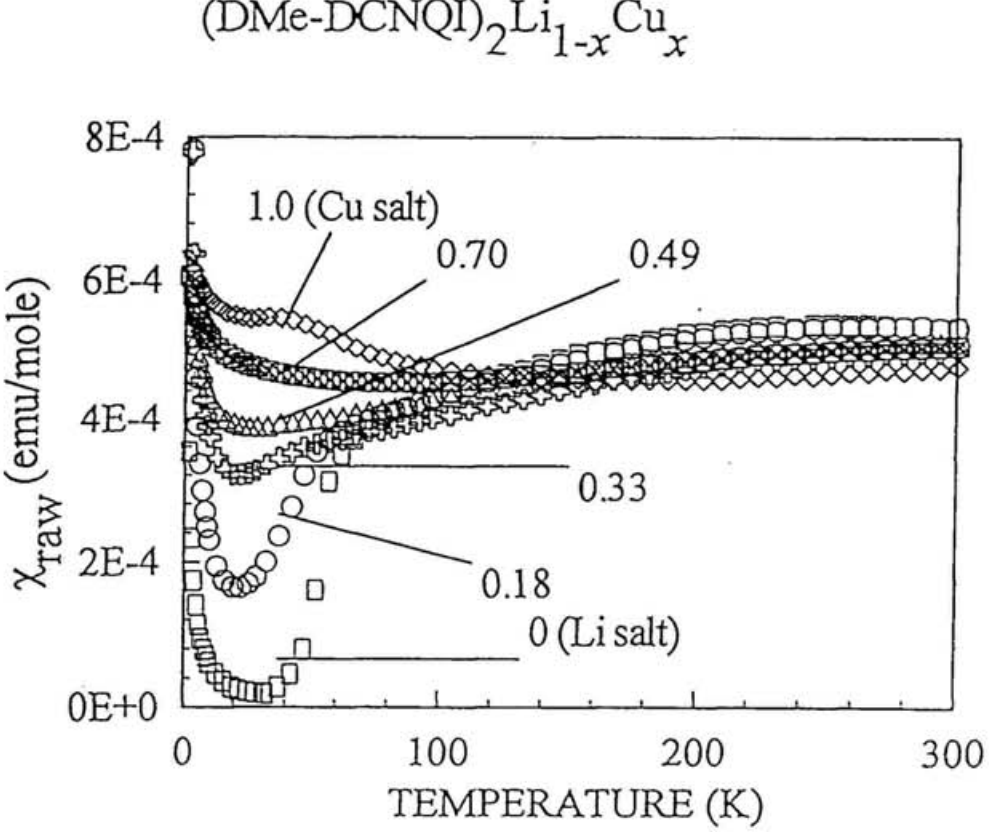

Fig. 4-3-3a) Temperature dependence of the raw data of χ.

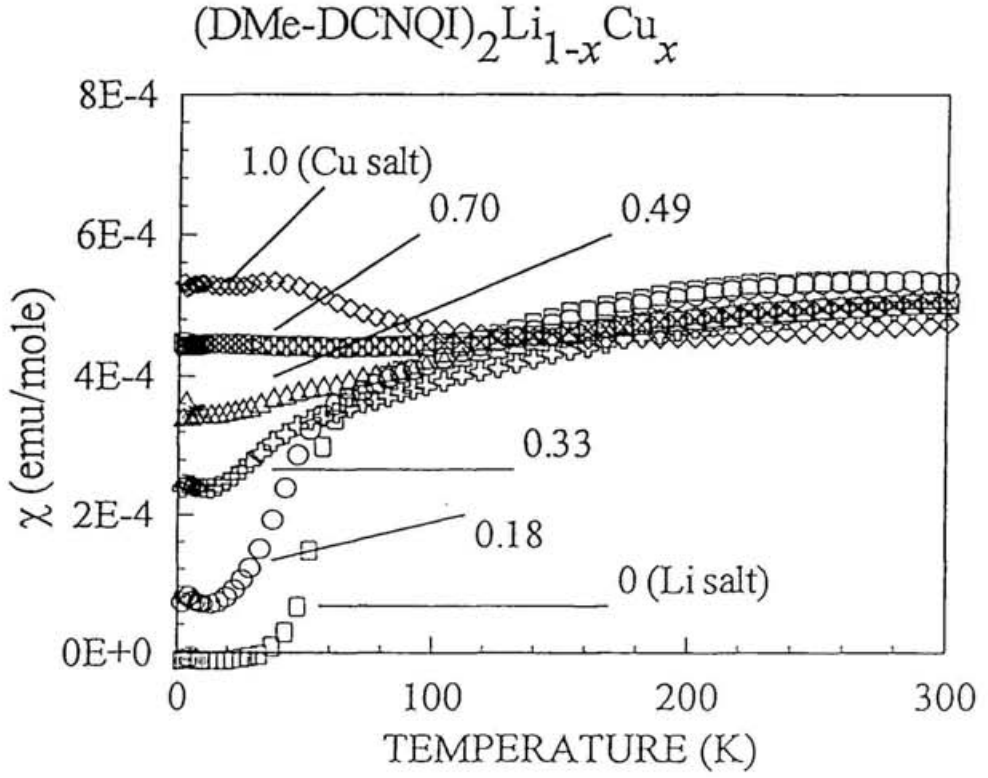

Fig. 4-3-3b) The Curie term subtracted data of χ.

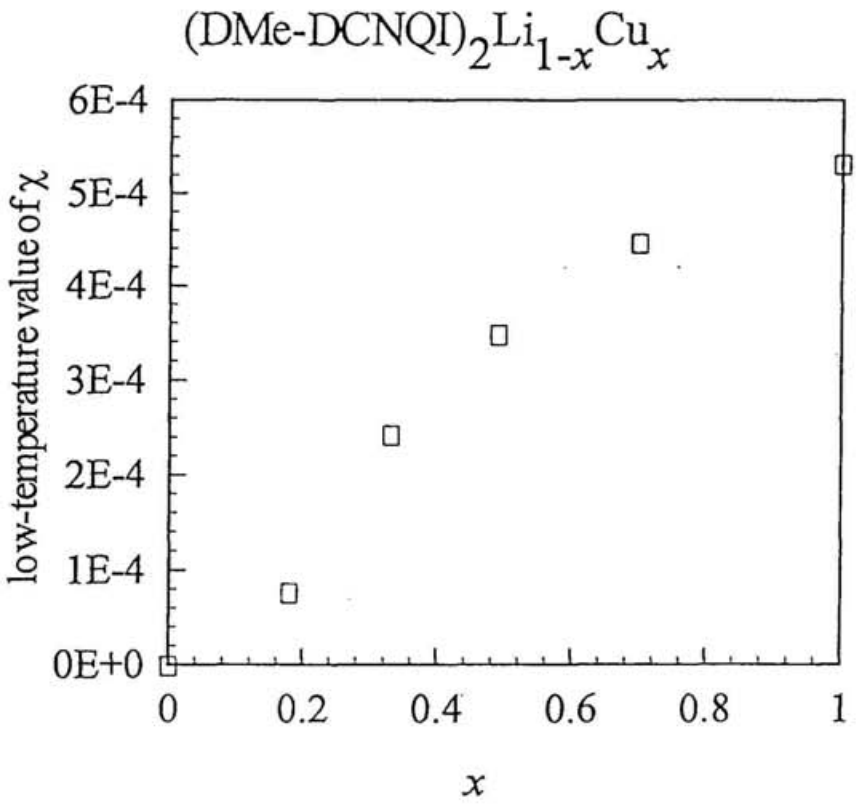

Fig. 4-3-4 Relationship between x and finite low-temperature value of χ.

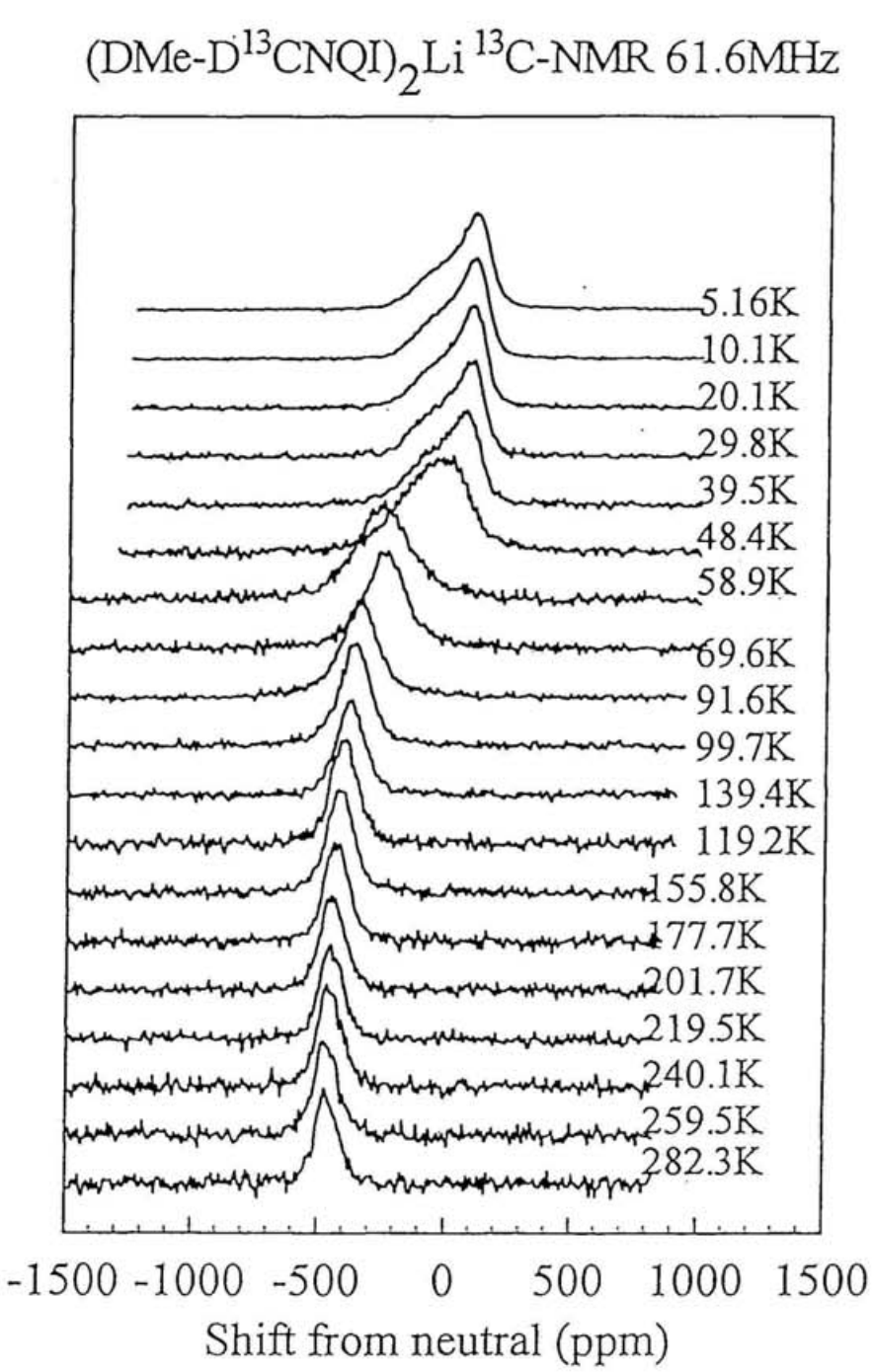

Fig. 4-4-1a) ^{13}C-NMR spectra of $x = 0$ system (Li salt).

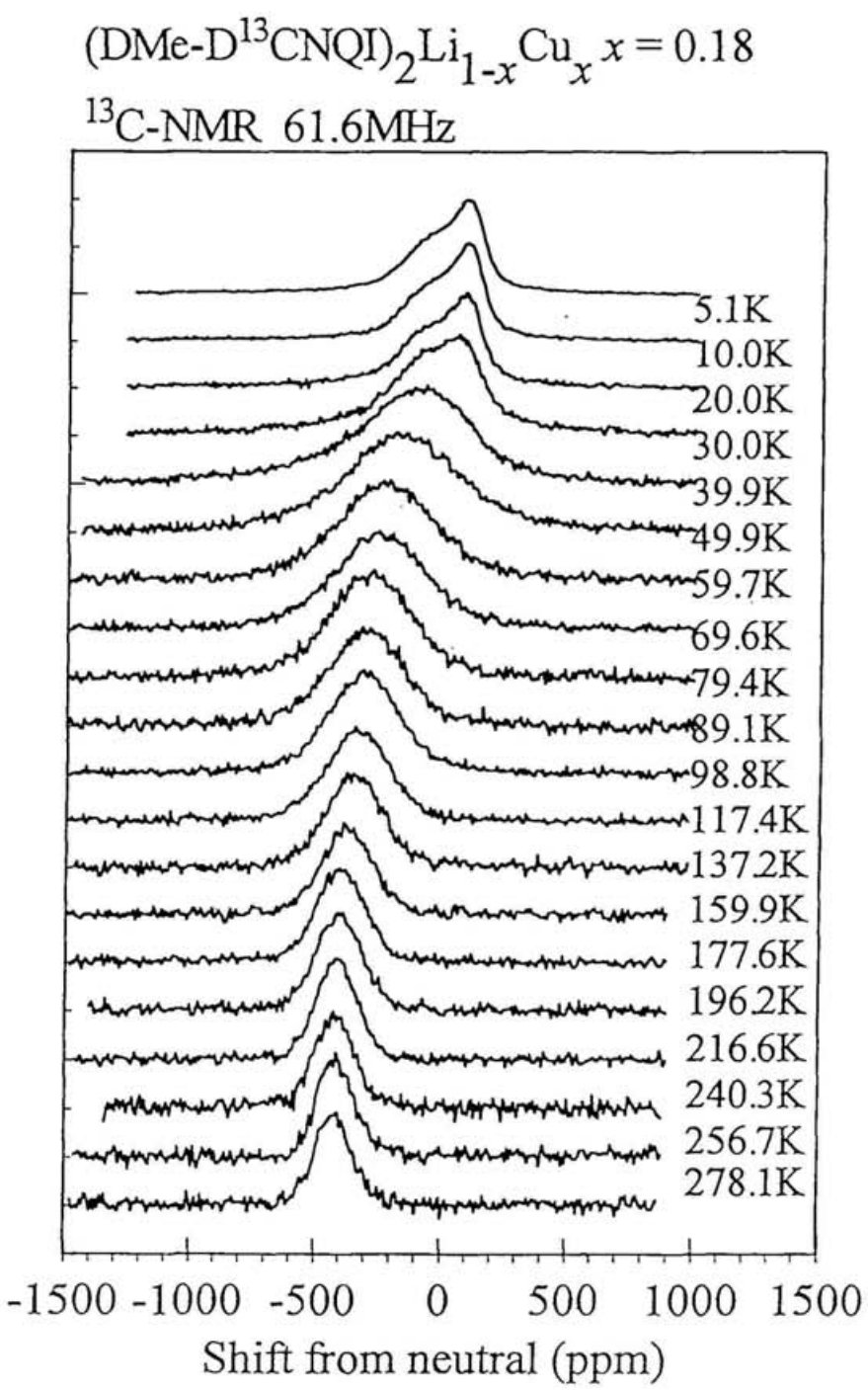

Fig. 4-4-1b) ^{13}C-NMR spectra of x=0.18 system.

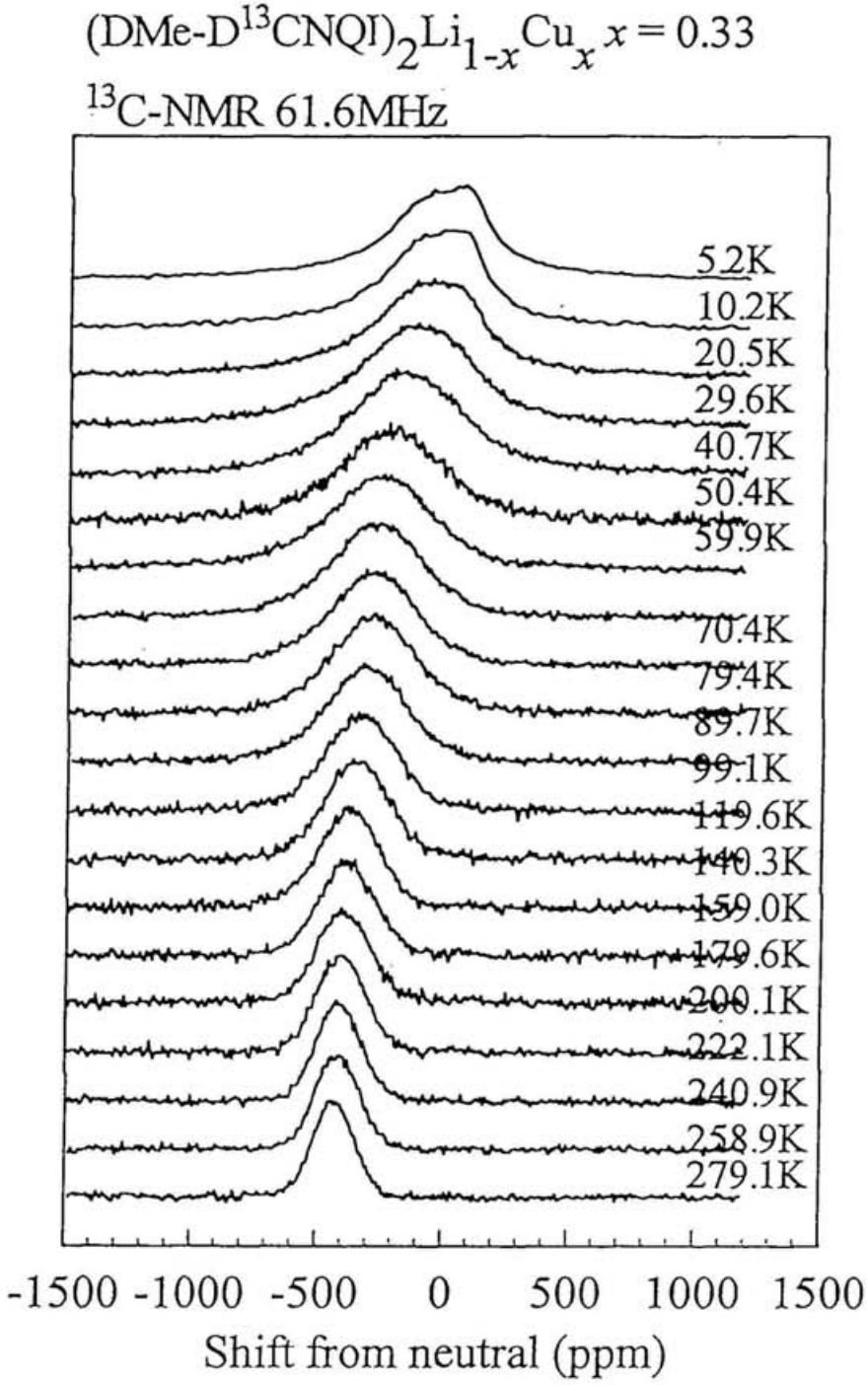

Fig. 4-4-1c) ^{13}C-NMR spectra of x = 0.33 system.

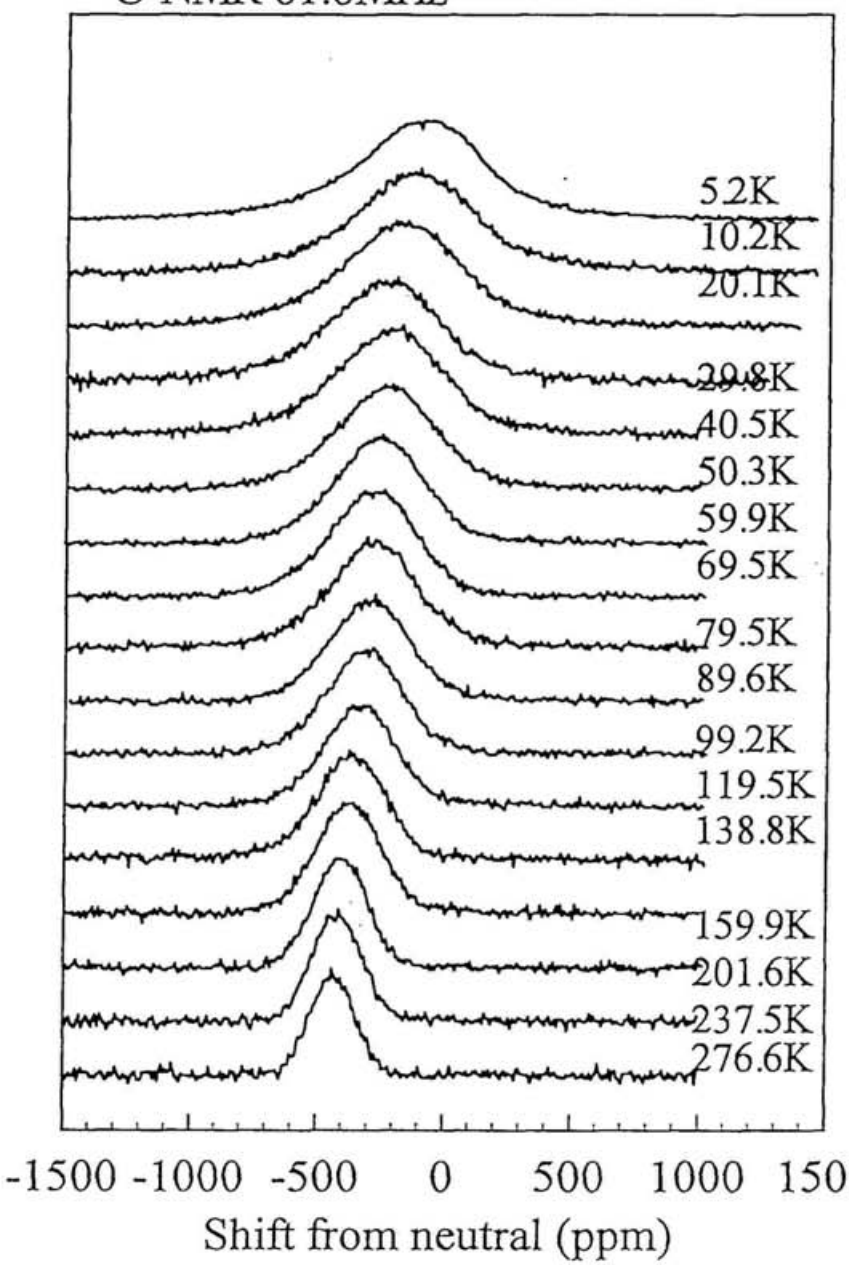

Fig. 4-4-1d) ^{13}C-NMR spectra of x = 0.49 system.

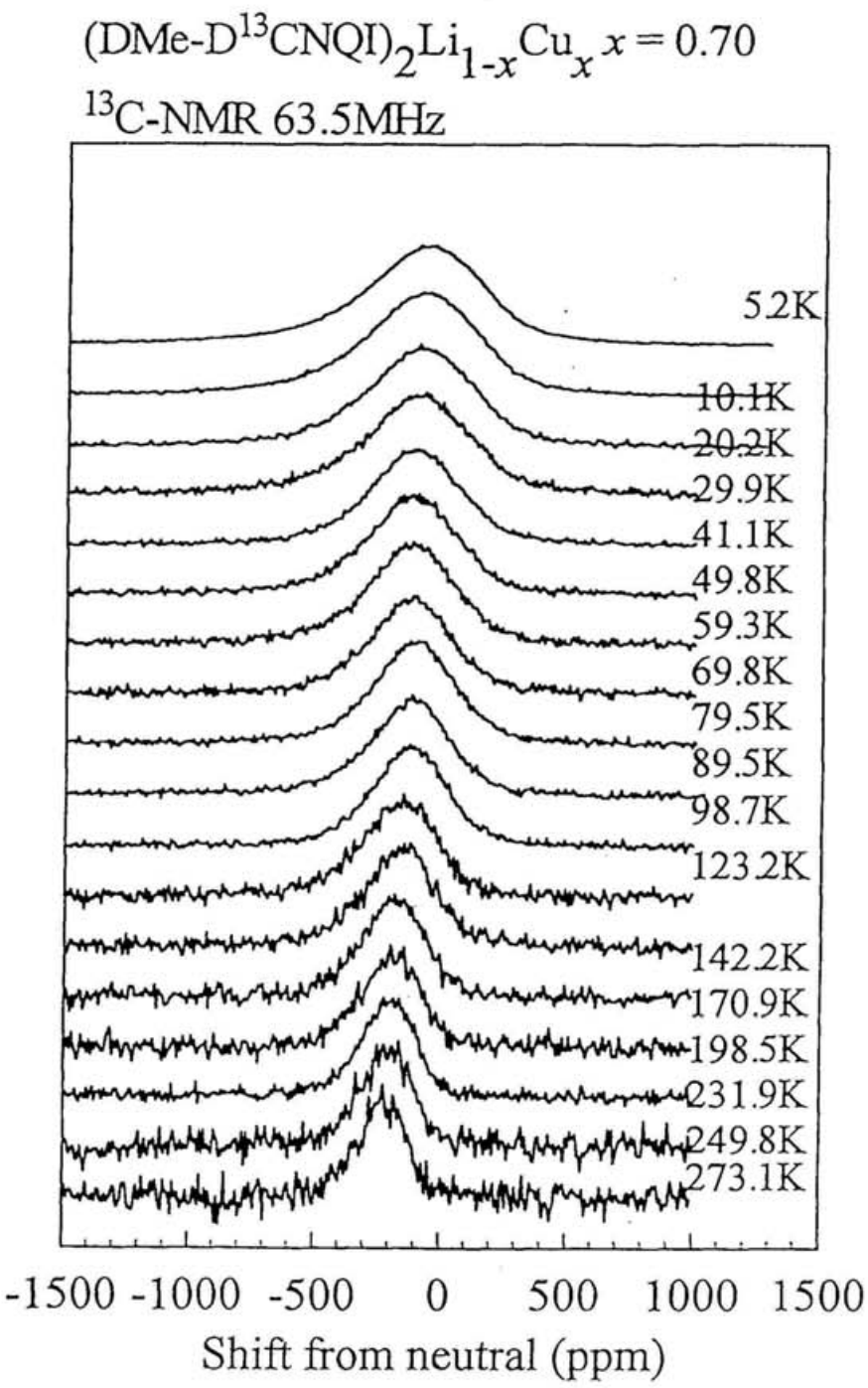

Fig. 4-4-1e) ^{13}C-NMR spectra of x = 0.70 system.

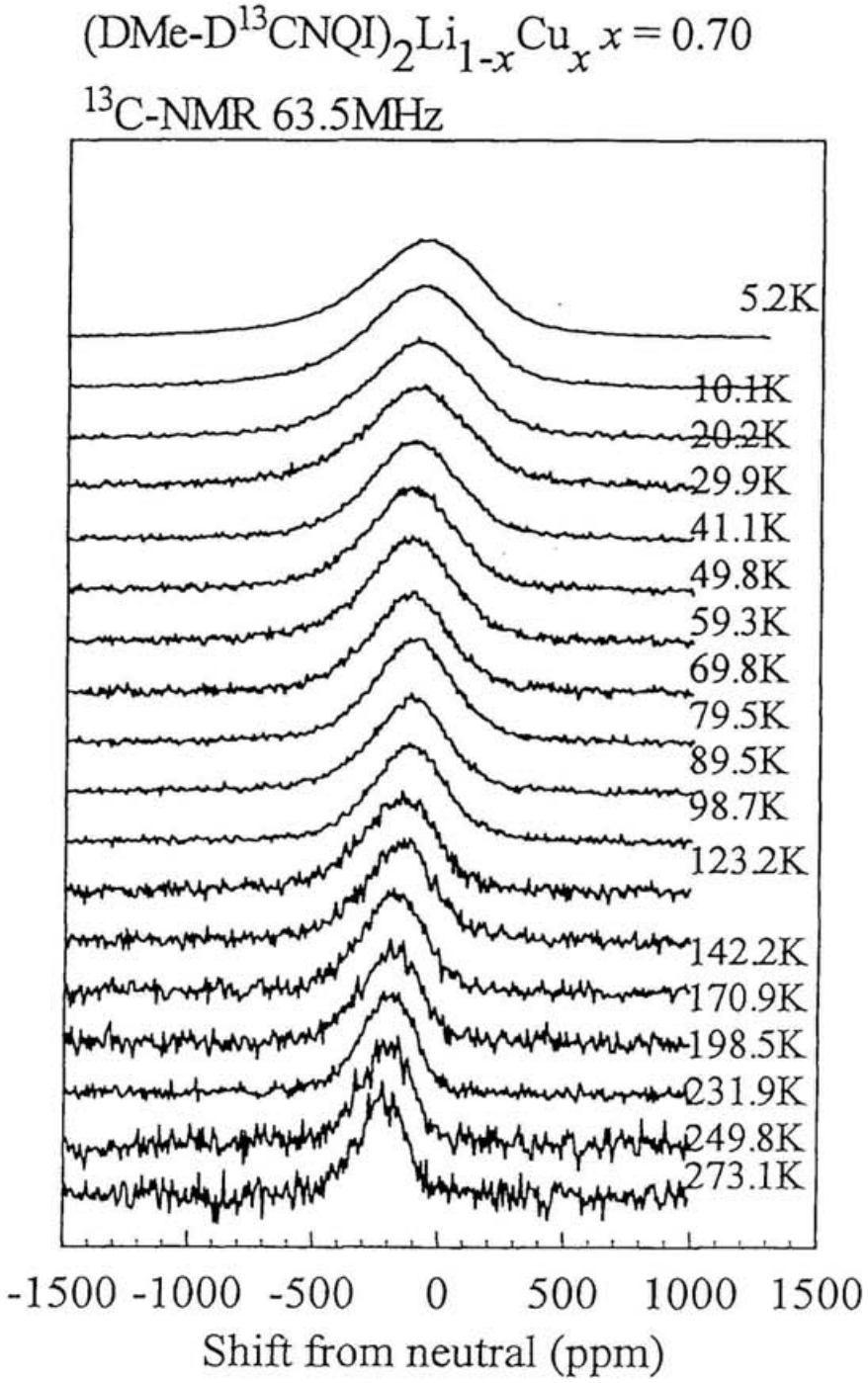

Fig. 4-4-1e) ^{13}C-NMR spectra of x = 0.70 system.

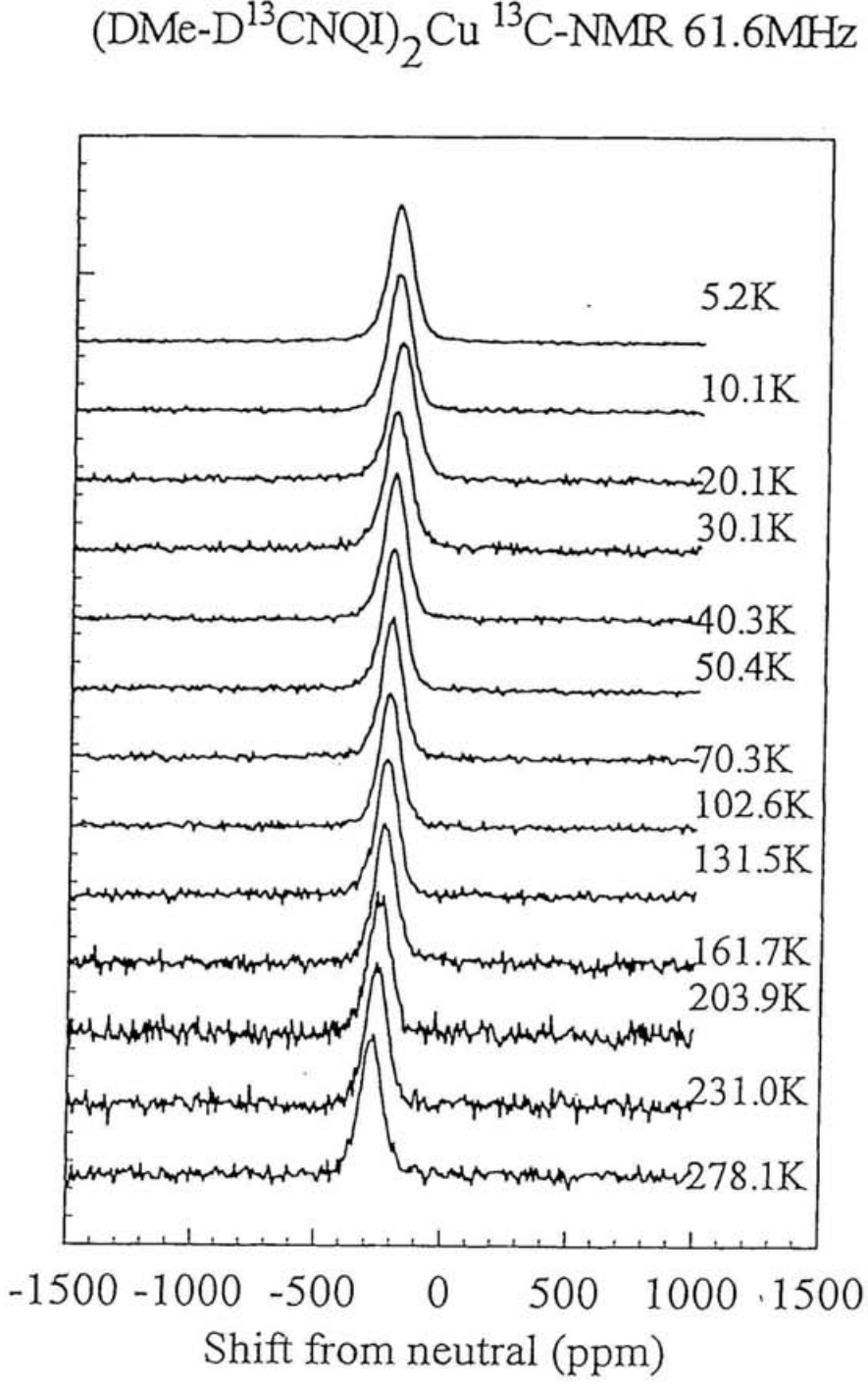

Fig. 4-4-1f) ^{13}C-NMR spectra of $x = 1$ (Cu salt) system.

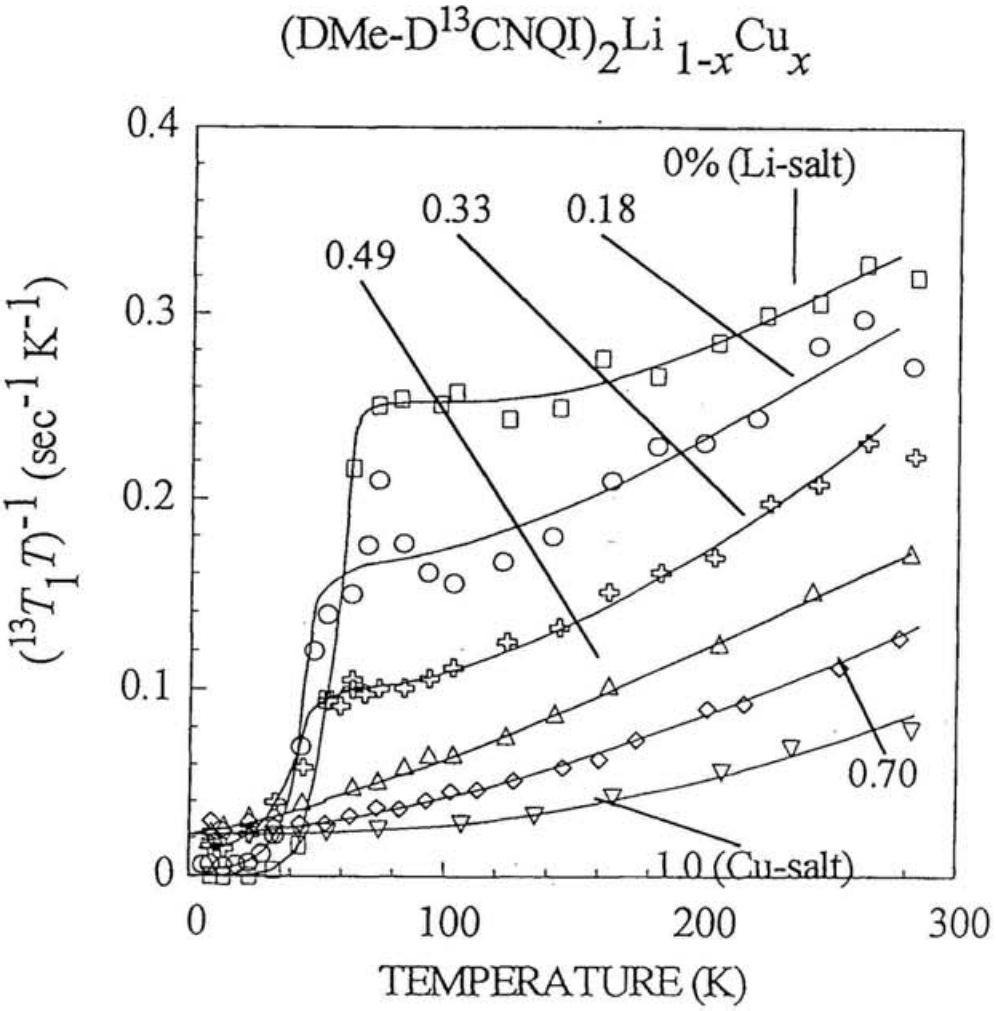

Fig. 4-4-2 temperature depndence of $(T_1 T)^{-1}$ of each system. Solid curves are guides to eyes.

Concluding remarks

The new electronic phases in DCNQI-Metal complexes have been developed and examined. By replacing the substitutents of DCNQI from Me to iodine, the electron correlation effect of the system become large. The newly synthesized $(DI\text{-}DCNQI)_2Ag$ was expected to afford nearly pure π electron system without π-d hybridization like isostructual $(DMe\text{-}DCNQI)_2Ag$. However, their electronic properties were found to be quite different from each other. DI-Ag is an insulator below room temperature. The $4k_F$ CDW with twofold charge ordering along the *c*-axis has been identified by the line separation of ^{13}C-NMR spectra. It is emphasized that the CDW is the charge modulation type rather than the lattice modulation type. The ground state of DI-Ag was found to be antiferromagnetic from NMR measurements and is a sharp contrast to the nonmagnetic (spin-) Periels state in DMe-Ag. DI-Ag is the first π electron antiferromagnet among the DCNQI-Metal complexes. The fundamentals of the electronic properties of DI-Li is similar to DI-Ag. The difference of the electronic state between DI-Ag/Li and DMe-Ag/Li is understood in terms of difference of the band width and the dimensionality of the electronic system. When Ag is replaced by Cu, the d orbital of Cu is hybridized to the π orbital in DCNQI at least for the DMe-system. We can imagine the same situation in the DI-system. It was observed that temperature dependence of ^1K, ^{13}K and χ_{spin} are different from one another. This provides an evidence that DI-Cu is a multi-band system constructed through the hybridization between π and d orbital.

The alloy systems, $(DMe\text{-}DCNQI)_2Li_{1-x}Cu_x$, have been synthesized. The band filling of DMe-DCNQI 1D π band and three dimensionality through the Cu 3d orbital have been

controled by the Cu doping in the Li site. In a lightly dope region ($x < 0.3$), the Cu doping gives the incomplete (spin-) Peisrls transition with finite values of susceptibility remaining at low temperatures. The systems with $x > 0.5$ behave metallic in whole temperature range. The resistivity, susceptibility and NMR behaviors lead us to consider that the insulator-metal transition or crossover around $x = 0.3$ is driven by the interplay between dimensional crossover of the electronic structure and disorder-induced electron localization. In this sense, disorder plays an important role in determining the electronic phases as well as dimensionality and band-filling. ^{13}C-NMR relaxation of all the systems in the metallic states ($T > 100$ K) indicates that the doping causes some change in the electronic states, particularly in excitation spectrum visualized in higher temperature region.

Appendix

The synthesis process of ^{13}C isotope substitution

Each DCNQI molecule was synthesized from the reaction of corresponding benzoquinone and bis(trimethylsilyl)carbodiimide ($(Me_3SiN)_2C$) in dichloromethane (CH_2Cl_2) as shown in Scheme 1[1,2] . The center carbon of bis(trimethylsilyl)carbodiimide is to be situated cyano carbon in the DCNQI molecule. The synthesis process of ^{13}C enriched bis(trimethylsilyl)carbodiimide is described in this section.

There are three steps of reactions as[3]

$$K^*CN + Br_2 \rightarrow Br^*CN + KBr \qquad (I)$$

$$Br^*CN + 2NH_3 \rightarrow H_2N^*CN + NH_4Br \qquad (II)$$

$$H_2N^*CN \xrightarrow[Et_2O]{Et_3N,\ Me_3SiCl} (Me_3SiN)_2{}^*C \qquad (III)$$

Step I

The water solution of K*CN (Isotec, 99.4% ^{13}C) (10g of K*CN / 55g of water) was dropped into a stirred mixture of 23.4 g (146.7 mmole) of brimine (Br_2; Nakarai GR) in the ice-bathed three necked flask for about two hours. It should be note that the temperature in the flask should be lower than ~ 10 ℃. About 15 minutes after, the distill head was put on the three necked flask. The distillation was carried out in the oil bath at ~ 80 ℃ (b. p. is 61℃, m. p. is 52℃). An amount of 11.98 g (112mmole, 74%) Br*CN

was yield based on K*CN.

The yield Br*CN was solved in ether and dried by $CaCl_2$ for the next step[4] .

Step II[5]

The 200 ml of the 2.0 M ammonia alcohol solution (Aldrich) was added dropwise to a stirred suspension of Br*CN obtained in the Step I in dry ether (~ 200 ml). The mixture was left overnight in a refrigerator. The filtered, and filtrate is evaporated to dryness under vacuum; yield 4.8 g (112 mmle 96% based on Br*CN).

Step III

25.3 g of Me_3SiCl (TCI-GR: 224 mmole) was added dropwise to stirred 22.7 g of Et_3N (Nakarai-GR; 224mmole) in a ice-bathed nitrogen-substituted three necked flask, and 60 ml of the dry ether was also added. The ether solution (60 ml) of H_2N*CN obtained at Step III was added dropwise to the flask for about an hour. The mixture was left for ~ 3 hours and filtered. The filtrate was evaporated and distilled (b. p. 83℃/500 torr); yield 11.2 g, 59.8 mmole, 39.5% based on K*CN.

---

[1] A. Aumüller and S. Hünig , Angew. Chem. Int. Ed. Engl. **23** (1984) 447

[2] A. Aumüller and S. Hünig, Liebigs Ann. Chemd. **1986** (1986) 142

[3] Hartman and Deger, Org. Synth.. **11**, (1931) 30

[4] Since BrCN does not keep well, it is preferable to prepare it just before using, The drying agent is not filtered off because of the appreciable vapor pressure of the product.

[5] S. Graff *et al.*, Canter research, **11**, (1951) 388

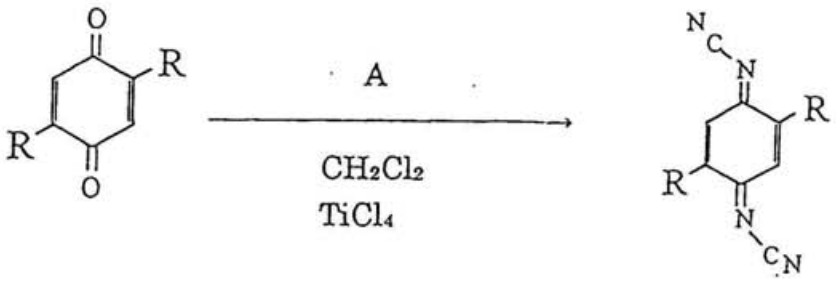

Scheme 1. Synthesis method of DCNQI molecule.[1]
A = $(Me_3SiN)_2C$.